Received: 13 May 2025 | Accepted: 1 October 2025

DOI: 10.1002/vzj2.70056

Vadose Zone Journal

ORIGINAL ARTICLE

Modeling saffron corm production under climate change using Hydrus-1D enhanced with a novel crop yield module

Amir Akbari[1] | **Ali Naghi Ziaei**[1,2] | **Seyed Mohammadreza Naghedifar**[1] | **Jan W. Hopmans**[3] | **Jamile Gholipour**[1]

[1]Department of Water Science and Engineering, College of Agriculture, Ferdowsi University of Mashhad (FUM), Mashhad, Iran

[2]Saffron Institute, University of Torbat Heydarieh, Torbat Heydarieh, Iran

[3]Department of Land, Air and Water Resources, University of California, Davis, Davis, California, USA

Correspondence
Ali Naghi Ziaei, Department of Water Science and Engineering, College of Agriculture, Ferdowsi University of Mashhad (FUM), Mashhad, 9177948974, Iran. Email: an-ziaei@um.ac.ir

Assigned to Associate Editor Christophe Darnault.

Funding information
Saffron Institute, University of Torbat Heydarieh, Torbat Heydarieh, Iran, Grant/Award Number: 179755

Abstract

Saffron (*Crocus sativus* L.) is an ideal crop for arid and semiarid regions due to its low water requirement and high economic value. This study involves calibration and validation of the Hydrus-1D model in order to explore the influence of climate change on saffron corm production. The research was carried out during the 2021–2022 and 2022–2023 growing seasons, focusing on 2-year-old and 3-year-old saffron, respectively, during which high-resolution in situ data were measured for soil water content, salinity, and soil temperature. Results showed that Hydrus-1D accurately simulated soil water content and temperature over two growing seasons. The root mean square error of simulations for soil water content and soil temperature was 0.034 cm^3/cm^3, 1.43°C, and 0.027 cm^3/cm^3, 1.54°C for the first and second growing seasons, respectively. However, the model provided an acceptable simulation of soil salinity in the first season. As Hydrus-1D does not inherently account for aboveground crop simulation, a new module based on the hybrid grey wolf optimizer and trust region algorithm was integrated to Hydrus-1D to simulate the saffron corm production. Using the new module with the three climate models including MRI-ESM2-0, ACCESS-CM2, and MIROC6 from Coupled Model Intercomparison Project Phase 6 under the Shared Socioeconomic Pathways (SSPs) SSP126, SSP245, and SSP585, the impact of climate change on saffron corm production in Mashhad-Iran during the near future (2025–2050) was evaluated. The results indicated that, during 2025–2050, climate change is not expected to negatively impact corm production in Mashhad-Iran, indicating the region's sustainability for saffron cultivation.

Abbreviations: AICc, corrected Akaike information criterion; ANOVA, analysis of variance; BIC, Bayesian information criterion; CCC, concordance correlation coefficient; CMIP6, Coupled Model Intercomparison Project Phase 6; DM, distribution mapping; EC, electrical conductivity; GCM, global climate model; GWO, grey wolf optimizer; LAI, leaf area index; LS, linear scaling; MAE, mean absolute error; NSE, Nash–Sutcliffe efficiency; RMSE, root mean square error; SSP, Shared Socioeconomic Pathway; TDR, time domain reflectometry; TR, Trust Region.

This is an open access article under the terms of the Creative Commons Attribution License, which permits use, distribution and reproduction in any medium, provided the original work is properly cited.
© 2025 The Author(s). *Vadose Zone Journal* published by Wiley Periodicals LLC on behalf of Soil Science Society of America.

Plain Language Summary

This paper investigates the impact of climate change on saffron corm production in Mashhad-Iran using the Hydrus-1D model. In this study, we calibrated and validated the Hydrus-1D model for saffron cultivation using high-resolution in situ data on soil water content, soil temperature, and soil salinity. Because Hydrus-1D could not simulate crop yield, we integrated a new yield simulation module optimized with the hybrid grey wolf optimizer and trust region algorithm. Finally, we used data from the Coupled Model Intercomparison Project Phase 6 climate models to assess the impact of climate change on saffron corm production through simulations with the Hydrus-1D model in Mashhad-Iran. Our results indicate that the region is expected to remain sustainable for saffron cultivation in the near future.

1 | INTRODUCTION

Saffron (*Crocus sativus* L.) is a perennial crop that falls under the Iridaceae family (Akramiani et al., 2024), holding the title of "red gold" in various countries spanning Asia, Europe, and Australia (Mehmeti et al., 2024). It is also considered the most valuable spice around the globe (Abbasi & Sepaskhah, 2023). Given the inevitable global water shortage, saffron, with its low water requirements and significant economic value, emerges as an ideal crop for cultivation in arid and semiarid regions experiencing hot summers and cold winters (Darvish et al., 2022; Moshizi et al., 2023). Iran has a long-standing tradition of saffron cultivation, being the leading producer and exporter of this valuable spice worldwide, accounting for about 90% of global saffron production (Bazrafshan et al., 2019). Due to Iran's water scarcity and the fact that 85% of the countries land area is classified as an arid or semiarid region (Rastegaripour et al., 2024), saffron cultivation may offer a valuable solution to save water resources.

Predicting crop yield is crucial for making strategic decisions in agriculture and is vital for effective water management (Bali and Singla, 2022). In the context of crop growth simulation, many crop parameters are involved, which collectively influence the growth and development of crops (Zhuo et al., 2022). Soil properties and meteorological data are crucial factors in this regard (Yi et al., 2022). Crop models such as WOFOST (Van Diepen et al.,1989), CROPSYST (Stöckle et al., 2003), AquaCrop (Steduto et al., 2009), EPIC (Williams et al., 1989), and DSSAT (Jones et al., 2003) have attempted to mimic the process of crop growth. However, their ability to accurately simulate soil temperature changes across the soil profile remains a limitation. More specifically, among the abovementioned models, WOFOST, CROPSYST, and AquaCrop cannot simulate soil temperature. Although EPIC and DSSAT simulate soil temperature using empirical equations, they do not solve the transient partial differential equations of heat transport. While more physically based models such as Hydrus-1D, which rely on numerical solutions of the Richards' equation, simulate transient heat transfer (Ventrella et al., 2019), their crop growth engine commonly lacks a thorough mechanistic algorithm (Chen et al., 2019).

There have been limited studies on the mechanistic modeling of saffron growth supported by high-resolution datasets. Sepaskhah et al. (2013) presented a dynamic model for predicting saffron yield, demonstrating their model's accuracy in estimating both saffron yield and corm production. Nevertheless, this model lacked sufficient accuracy to simulate parameters such as soil water content and leaf area index (LAI), which are crucial indicators for estimating transpiration and crop yield. Mirsafi et al. (2016) showed, for the first time, that the AquaCrop model can accurately predict saffron biomass in early years. They also concluded that the AquaCrop model is capable of simulating the variations of soil water content and can serve as an effective tool for simulating the growth of perennial crops. However, the soil water content was measured only once in each growing season, thus being inadequate for model calibration. Akbari et al. (2024) utilized high-resolution data and calibrated the AquaCrop model to examine the impact of water movement on saffron growth. These improvements allowed Akbari et al. (2024) to accurately simulate saffron growth stages, but the study did not take into account the effects of salt dynamics and heat transfer. Despite saffron's sensitivity to soil temperature, no studies have used physically based models such as Hydrus-1D to simulate its growth under varying soil temperature and salinity conditions.

The success of saffron production relies significantly on favorable environmental conditions (Wang, Li, Xu, et al., 2021), among which air temperature plays a critical role. There have been few studies investigating the impact of temperature on saffron production. Molina et al. (2005) found through experiments in controlled environments that air temperature significantly influences saffron flowering, with the

average daily temperature being the most crucial environmental factor in describing its flowering behavior. Koocheki et al. (2007) demonstrated that the primary environmental factor impacting saffron growth is the daily temperature, with an optimal range of 9°C–17°C. Gresta et al. (2009) discovered that to initiate saffron flowering, a specific combination of temperature and soil water content is essential. According to Cardone et al. (2019), optimum stigma yield (28.1 kg/ha) with high quality is achievable for places characterized by higher temperatures, while the flowering period remained unaffected by excessive rainfall. Akbari et al. (2024) by using the AquaCrop model examined the impact of air temperature on saffron corm across various regions in Iran and determined that saffron is more sensitive to freezing than to heat. However, this study did not simulate the temperature of the saffron root zone. None of the studies investigates the impact of climate change. Since AquaCrop lacks the capability to predict soil temperature, modeling soil temperature variations alongside crop production using AquaCrop is not feasible.

The novelty of this paper aligns with its primary objectives, which aim to bridge the abovementioned gaps. More specifically, the Hydrus-1D model was calibrated and validated using high-resolution in situ measurements of soil temperature, soil water content, and electrical conductivity (EC) of soil solution in a 2-year study on saffron. Furthermore, a new module based on a hybrid grey wolf optimizer–trust region (GWO–TR) optimization algorithm has been developed to enhance Hydrus-1D for yield simulation. Finally, Coupled Model Intercomparison Project Phase 6 (CMIP6) climate projections under three emission scenarios SSP1-2.6, SSP2-4.5, and SSP5-8.5 were used to examine the impact of climate change on saffron yield in the study area during 2025–2050.

Core Ideas

- Hydrus-1D was calibrated and validated using high-resolution soil data for saffron fields.
- A new yield module simulated saffron corms using the grey wolf optimizer and trust region methods.
- Three Coupled Model Intercomparison Project Phase 6 models assessed saffron response to climate change through 2050.
- Climate change is unlikely to reduce saffron corm yield in Mashhad by 2050.

2 | MATERIALS AND METHODS

2.1 | Site description

The field study was carried out over two consecutive years, from 2021 to 2023, at the research farm of Ferdowsi University of Mashhad (FUM), Mashhad, Iran. This region is semiarid and receives an average of 250 mm of precipitation annually (Sharafkhane et al., 2024). The farm is located at 36°16′ N, 59°36′ E, and is 985 m above mean sea level (Figure 1). In September 2020, saffron was planted in rows in a 0.5-ha field at FUM. The presented experiment was conducted for 2-year- and 3-year-old saffron corms. The corm of the saffron plant resembles a small bulb underground, formed from a specialized section of the plant stem by which it reproduces. Each corm yields purple flowers with grass-like leaves and yellow stamens. The flowers have three bright red stigmas, which are harvested and dried to produce saffron. The corms were planted in rows that were 50 cm apart, with an average distance of 25 cm between the corms on each row, resulting in a plant density of 100 corms per m^2. In the first year, the experimental field was irrigated using a rain hose sprinkler, while it was irrigated using drip tape irrigation in the second year. In this study, irrigation was applied based on farmers' experience and conventional local practices, reflecting real on-farm conditions rather than fixed experimental protocols. The meteorological station at 400 m away from the study area provided daily data on precipitation, maximum and minimum temperature, and wind speed during crop growth. The quantity of irrigation and precipitation during the 2-year experiment is presented in Figure 2. A flow meter was used to measure the depth of irrigation water. Figure 2 also shows the maximum, mean, and minimum temperatures, recorded automatically every 10 min.

Three soil samples were randomly collected from 0- to 10-cm, 10- to 20-cm, 20- to 30-cm, and 30- to 60-cm layers to measure soil hydraulic characteristics and soil textural properties in the laboratory. Bulk density was measured using three undisturbed soil samples, which were collected from the soil layers using a cylindrical soil sampler. The soil texture was determined using the hydrometer method (ASTM-H152), under Bouyoucos' (1962) instructions. The falling head method was used to conduct the saturated hydraulic conductivity tests. The centrifuge method (Kokusan Ensinki Co., Ltd.) was used to measure soil moisture at saturation, field capacity, and the permanent wilting point. The average EC of irrigation water was measured at 1 ± 0.1 dS/m using a portable EC meter (Waterproof EC Tester Low, Eutech Instruments Pte, Ltd., ±0.01 ds/m). A time domain reflectometry (TDR) 350 soil moisture meter (Spectrum Technologies) monitored soil water content during the growing seasons, in addition to soil salinity and soil temperature across the 20-cm depth, about equal to the root zone depth, by way of 10 stations across the saffron field, diagonally. The accuracy of the TDR 350 probe was evaluated through comparison with standard reference methods. As shown in Figure 3a, volumetric soil moisture content determined by the gravimetric method

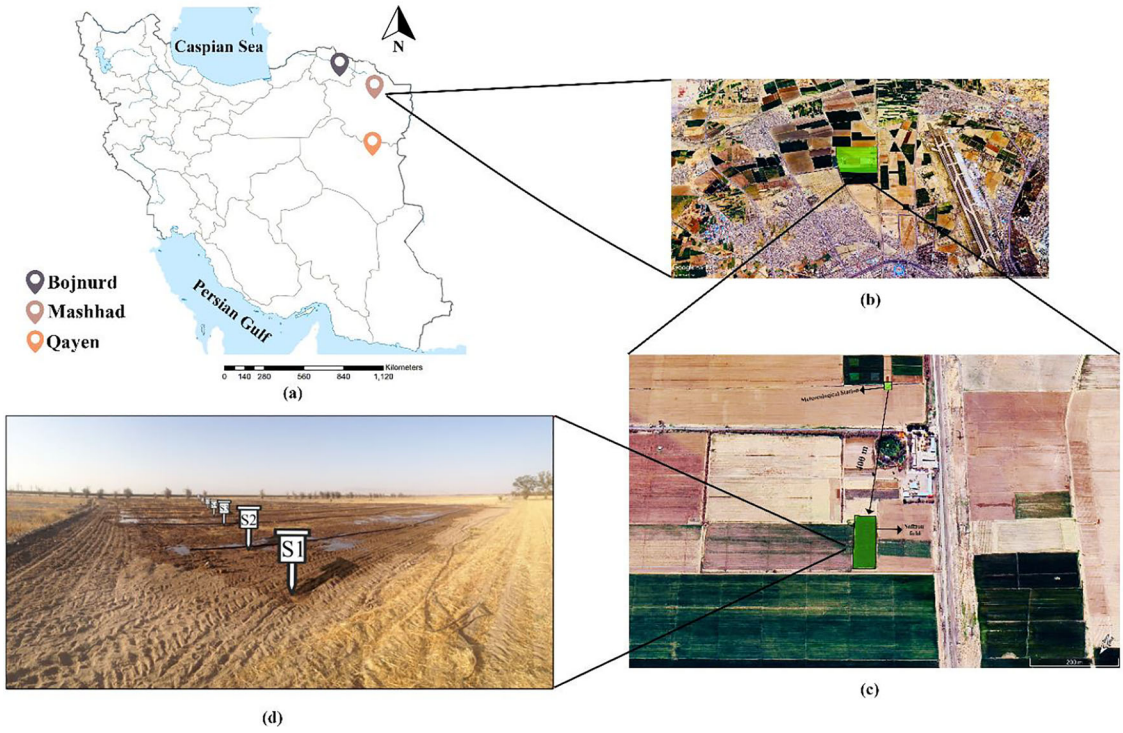

FIGURE 1 (a) Location of study areas in Iran, (b) research farm of Ferdowsi University of Mashhad, (c) aerial view of saffron field (experimental site), and (d) saffron field.

exhibited a strong linear correlation with the values measured by the TDR 350 ($R^2 = 0.96$) (Abedinpour et al., 2012). Similarly, EC values obtained using a standard EC meter were highly correlated with those measured by the TDR 350 ($R^2 = 0.98$) (Figure 3b), confirming the device's reliability for simultaneous monitoring of soil moisture and salinity. In addition, three 1-m^2 plots were selected in the field to monitor the saffron canopy cover with ImageJ software version 1.52, using a camera (Canon IXY 410F, resolution: 4011 × 3016, Canon Inc.). Six random corm samples were collected from the study area biweekly, from which the weight of daughter corms and aboveground biomass was measured after drying in an oven (70°C) for 24 h. These field samples were also used for measuring root depth and calculating the LAI. To calculate LAI, the leaves were taken to the laboratory, and their area was measured using Delta-T Devices WinDIAS (in cm^2).

2.2 | Model descriptions

Hydrus-1D software was used to simulate water flow, heat transfer, and salt transport (Šimůnek & van Genuchten, 2008). The mixed form of one-dimensional Richards' equation is as follows:

$$\frac{\partial \theta}{\partial t} = \frac{\partial}{\partial z}\left[K\left(\frac{\partial h}{\partial z} + 1\right)\right] - S \tag{1}$$

where h is soil water matric head [L], K is unsaturated hydraulic conductivity [L T^{-1}], t is time [T], z is spatial coordinate [L], and S is the sink term [L^3 L^{-3} T^{-1}] accounting for root water uptake. Constitutive functions of Van Genuchten (1980) are employed to describe the soil water retention curve and unsaturated hydraulic conductivity as follows:

$$S_e = \frac{\theta - \theta_r}{\theta_s - \theta_r} = \frac{1}{\left(1 + (\alpha h)^n\right)^m} \tag{2}$$

$$K(h) = K_s S_e^l \left(1 - \left(1 - S_e^{\frac{1}{m}}\right)^m\right)^2$$

$$\text{where } m = 1 - \frac{1}{n}, n > 1 \tag{3}$$

where θ_s is saturated water content [L^3 L^{-3}]; θ_r is residual water content [L^3 L^{-3}]; m [−], n [−], and α [L^{-1}] are empirical shape factors that are obtained in the fitting process; K_s is saturated hydraulic conductivity [L T^{-1}]; and l is the pore connectivity parameter, which is commonly assumed to be 0.5 [−].

Beer's law was employed to partition potential transpiration (Ritchie, 1972) as follows:

$$T_p = ET_p\left(1 - e^{-k \times LAI}\right) \tag{4}$$

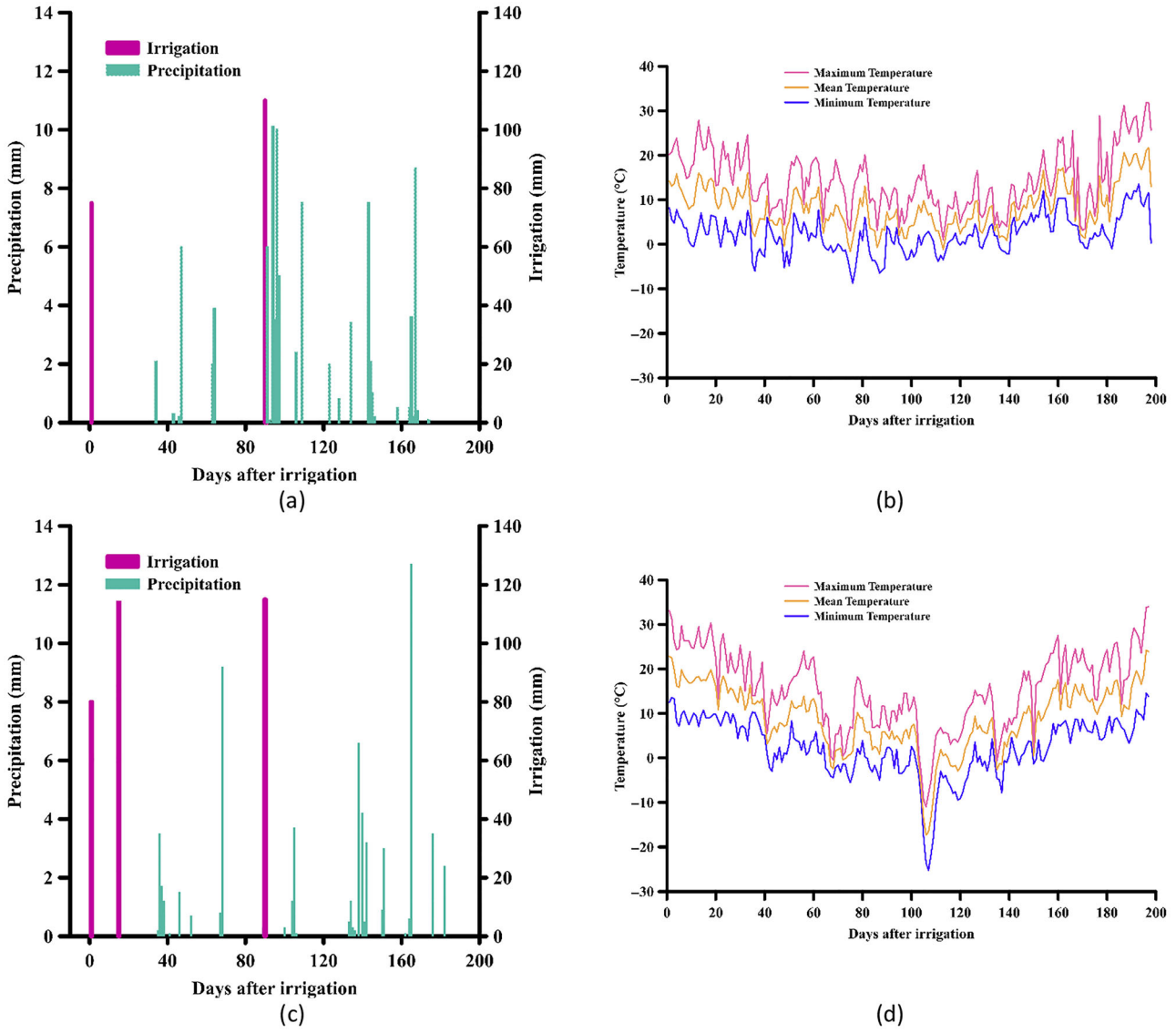

FIGURE 2 (a and c) Irrigation and precipitation (mm), alongside (b and d) temperature trends for the growing seasons of 2021–2022 and 2022–2023.

where T_p is potential crop transpiration [L T^{-1}]; ET_p is potential evapotranspiration [L T^{-1}]; LAI is leaf area index [−]; and k represents radiation extinction caused by the canopy, which is commonly equal to 0.39 [−] (Jiménez-Martínez et al., 2009; Šimůnek et al., 2008). According to Šimůnek and Hopmans's (2002) model, root water uptake is defined by the sink term S:

$$S(h) = \alpha(h) \times b(z,t) \times T_p \tag{5}$$

where $\alpha(h)$ is the soil water stress response function [−] and $b(z,t)$ is the normalized water uptake distribution function [L^{-1}]. The water stress function of Feddes et al. (1978) was defined as follows:

$$\alpha(h) = \begin{cases} \frac{h-h_4}{h_3-h_4}, & h_4 < h \le h_3 \\ 1, & h_3 < h \le h_2 \\ \frac{h-h_1}{h_2-h_1} & h_2 < h < h_1 \\ 0, & h \le h_4 \text{ or } h > h_1 \end{cases} \tag{6}$$

where the matric potential head is represented by parameters h_1 to h_4. The stress response function peaks between pressure heads h_2 and h_3, while linearly decreases to 0 above h_1 (due to oxygen deficiency) and below h_4 (because of the suction at the wilting point).

Actual transpiration (T_a) is calculated through Equation (7):

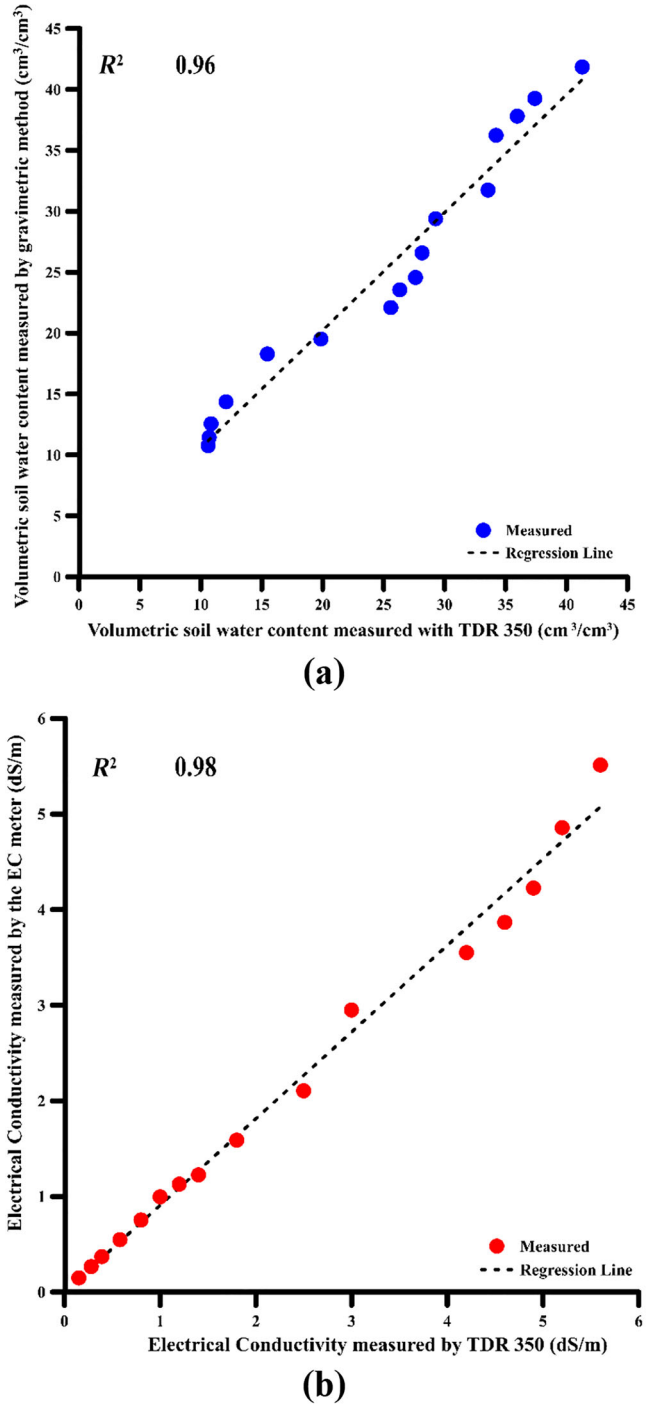

FIGURE 3 (a) Relationship between volumetric soil water content measured by the gravimetric method and by the time domain reflectometry (TDR) 350; (b) relationship between electrical conductivity (EC) measured by a standard EC meter and by the TDR 350.

$$T_a = T_p \int_{L_R} \alpha(h)\, b(z,t)\; dz \tag{7}$$

The dynamic root depth L_R[L], was calculated as the product of maximum rooting depth (L_m [L]) and root growth coefficient (f_r [−]) (Šimůnek & Suarez et al., 1993), computed as follows:

$$f_r(t) = \frac{L_0}{L_0 + \left(L_m + L_0\right) e^{-rt}} \tag{8}$$

where L_0 is the initial value of the rooting depth at the beginning of the growing season [L] and r is the growth rate [T^{-1}]. The growth rate is determined by assuming that 50% of the rooting depth will be attained after 50% of the growing season has passed. Due to the available data, the growth rate was determined by the in situ measurements.

2.2.1 | Solute transport

The Hydrus-1D solves the advection–dispersion equation (ADE) to describe the solute transport and heat transfer in soil. The equations for solute transport in Hydrus-1D advection and dispersion, as well as diffusion (Šimůnek & van Genuchten, 2008).

$$\frac{\partial \theta C}{\partial t} + \rho \frac{\partial s}{\partial t} = \frac{\partial}{\partial t}\left(\theta D \frac{\partial C}{\partial z}\right) - \frac{\partial qC}{\partial z} \tag{9}$$

where C is the solute concentration [M L^{-3}], D is the effective dispersion coefficient [L^2 T^{-1}], q is the volumetric fluid flux density, and s is the adsorbed concentration [M M^{-1}]. In this study, the adsorption is assumed to be governed by the linear equilibrium isotherms defined as follows:

$$s = K_d\, c \tag{10}$$

2.2.2 | Heat transfer

In the absence of water vapor diffusion, one-dimensional heat transfer can be modeled using the ADE as follows:

$$C_p(\varrho) \frac{\partial T}{\partial t} = \frac{\partial}{\partial z}\left[\lambda(\varrho) \frac{\partial T}{\partial z}\right] - C_w \frac{\partial qT}{\partial z} \tag{11}$$

where $\lambda(\varrho)$ represents the apparent thermal conductivity of the soil [ML T^{-3} K^{-1}], $C_p(\varrho)$ is the volumetric heat capacity of the porous medium [ML^{-1} T^{-2} K^{-1}], and C_w is the volumetric heat capacity of the liquid phase [ML^{-1} T^{-2} K^{-1}]. De Vries (1963) provides the equation for the volumetric heat capacity as follows:

$$C_p(\varrho) = \left(1.92\varrho X_n + 2.51\varrho X_o + 4.18\varrho\right) \times 10^6 \tag{12}$$

where ϱ is the volumetric fraction [L^3 L^{-3}], and the subscripts n, o, a, and w correspond to the solid phase, organic matter, gas phase, and liquid phase, respectively. The apparent thermal conductivity $\lambda(\varrho)$, which varies linearly with velocity, is

determined using the following equation (De Marsily, 1986):

$$\lambda\ (\varrho) = \lambda_0\ (\varrho) + \beta_t C_w\, |q| \tag{13}$$

where β_t represents the thermal dispersivity [L] and $\lambda_0(\varrho)$ is thermal conductivity, which explains the tortuosity of the porous material (Nakhaei & Šimůnek, 2014), described by Chung and Horton's (1987) equation as follows:

$$\lambda_0\ (\varrho) = b_1 + b_2\varrho + b_3\varrho X^{0.5} \tag{14}$$

Here, b_1, b_2, and b_3 are coefficients determined empirically.

2.3 | Model calibration and validation

2.3.1 | Hydrus-1D setup

Hydrus-1D simulations were carried out for soil water content, solute transport, and heat transfer in comparison with in situ observations. These simulations were run daily from October 2, 2021, to April 17, 2022, for the first growing season and from September 29, 2022, to April 13, 2023, for the second growing season. The soil profile was assumed to have a depth of 60 cm and was divided into four soil materials: 0–10 cm, 10–20 cm, 20–30 cm, and 30–60 cm. Since the probes of the TDR 350 device are 20 cm long, matching the planting depth of saffron, the observation points for the simulation were positioned in the Hydrus-1D at a depth of 20 cm. Therefore, 10 equal observation points were distributed from 0 to 20 cm. The average values of these 10 points were considered as the final data for comparison with the simulated values. However, to ensure that $\frac{\partial h}{\partial z} \cong 0$ in the water flow simulation, the soil depth was considered significantly deeper (60 cm) than the simulation points, likely representing the lower boundary of free drainage. Accordingly, the expected conditions for simulating solute transport and heat transfer are as follows:

$$\frac{\partial c}{\partial z} \cong 0 \text{ and } \frac{\partial T}{\partial z} \cong 0.$$

For the first year, the initial conditions of water flow and solute transport equations were defined based on field measurements taken on October 2, 2021, with soil water content, EC, and soil temperature of 0.32 cm^3/cm^3, 0.95 dS/m, and 22°C, respectively. For the second year, initial conditions were likewise set according to measurements on September 29, 2022, with corresponding values of 0.32 cm^3/cm^3, 0.75 dS/m, and 20°C. Upper and bottom water flow boundary conditions were atmospheric boundary conditions with surface layer and free drainage, respectively. The boundary conditions for salt transport were defined as the concentration flux of the infiltrating water at the upper boundary and zero concentration gradient at the lower boundary. For the heat transport simulations, the measured surface temperature was used for the upper boundary, and a zero temperature gradient was considered as the lower boundary.

2.3.2 | Physicochemical and thermal soil properties

Soil hydraulic parameters

The soil hydraulic parameters K_s and θ_s were measured in the laboratory, while the remaining parameters, including n, α, and θ_r, were estimated from soil retention data using the RETC software package (Van Genuchten et al., 1991). These parameters were derived using Van Genuchten's (1980) model, employing input data on soil percentage and bulk density.

Salt transport parameters and soil thermal parameters

As independently measuring all solute transport and heat transfer parameters in this study is challenging, several parameters must be estimated using field-measured soil temperature and soil salinity data along with an inverse method. The Hydrus-1D inverse feature is highly popular among users as it minimizes the need for multistep and time-consuming field measurements (Šimunek et al., 2012). This model employs a parameter estimation technique based on the Marquardt–Levenberg algorithm to minimize the errors between in situ measurement and simulation results (Marquardt, 1963; Šimůnek & Hopmans, 2002) in the objective function using least-squares optimization. This algorithm is employed for the inverse estimation of soil hydraulic properties, as well as solute transport and heat transfer parameters, based on measured data. Thus, the sensitive parameters were first identified manually, which included dispersion coefficient and adsorption isotherm coefficient for the salt transport equation, the thermal dispersivity, and thermal conductivity parameters (b_1, b_2, and b_3) for the heat transfer equation. Finally, these parameters were estimated using the inverse Hydrus-1D model, based on field measurements (soil salinity and soil temperature) taken during the first growing season (2021–2022). The optimization of the parameters was performed separately for solute transport and soil thermal properties. Within each group, the parameters were optimized simultaneously (i.e., solute transport and soil thermal parameters were each optimized collectively).

2.3.3 | Root water uptake parameters

The root water uptake parameters were derived from the study by Dastranj and Sepaskhah (2019), which investigated saffron's response to salinity and various irrigation regimes. Root

growth was also predicted using root depth measurements taken over the two growing seasons as input data.

2.4 | New module for calculation of saffron corm yield

The Hydrus-1D model cannot simulate crop yield and is limited to simulating actual evaporation and actual transpiration (Karandish & Šimůnek, 2019). To the best of the author's knowledge, for the first time, in this research, a module was developed and coupled with Hydrus-1D to simulate saffron corm yield. To this end, the parameters T_{cum} and Y_{rel} were first defined as follows: x

$$T_{\text{cum}} = \sum_{i=1}^{n} \frac{T_{\text{a}}}{\text{ET}_0} \tag{15}$$

$$Y_{\text{rel}} = \frac{\text{CY}_n}{\text{CY}_f} \tag{16}$$

where n is number of days after fist irrigation. Furthermore, $\sum_{i=1}^{n} \frac{T_a}{\text{ET}_0}$ represents cumulative daily transpiration to daily reference evapotranspiration, and $\frac{\text{CY}_n}{\text{CY}_f}$ denotes the ratio of corm yield on day n to the corm yield measured at the end of the growing season.

Corm yield was measured 10 times from the beginning of the first growing season (2021–2022) to the end. A newly developed crop yield function, inspired by the sigmoidal growth models of the Richard-type (Richards, 1959), was employed to fit the data. This is a function known for simulating crop growth. Equation (17) was presented to fit the data. Coefficients (M, d, a, b, and c) were added to the equation for more flexibility.

$$y = \frac{M}{d + \exp[-a\left(T_{\text{cum}} - b\right) + c]} \tag{17}$$

To obtain the best fit to Equation (3) with the data from the first growing season, a hybrid metaheuristic method developed by Selahvarzi et al. (2025) was employed. This approach is founded on the integration of the GWO and the TR algorithm.

The GWO is a swarm-based metaheuristic algorithm inspired by nature, mimicking the social hierarchy and hunting strategies of wolves. The performance of this algorithm reflects the cooperative hunting behavior of a pack of grey wolves, which gradually leads to the optimal solution by tracking, encircling, and attacking its prey (Wu et al., 2024).

According to their influence, grey wolves are categorized into four types: alpha (α), beta (β), delta (δ), and omega (ω). The algorithm's process is mathematically formulated as follows:

$$\vec{D} = \left|\vec{C} . \vec{X}_{\text{p}}(t) - \vec{X}(t)\right| \tag{18}$$

$$\vec{X}(t+1) = \vec{X}_{\text{p}}(t) - \vec{A} . \vec{D} \tag{19}$$

where $\vec{D}$ represents the updated position vector of the grey wolf, t is the current iteration, $\vec{X}_{\text{p}}$ is the vector of prey, $\vec{X}$ is the vector of grey wolves, and $\vec{A}$ and $\vec{C}$ are the vectors of coefficients.

The vectors A and C are determined using Equations (20) and (21) as follows:

$$\vec{A} = 2\vec{a} . \vec{r}_1 - \vec{a} \tag{20}$$

$$\vec{D} = 2 . \vec{r}_2 \tag{21}$$

$\vec{a}$ is determined using Equation (5).

$$\vec{a} = 2 - t\frac{2}{\text{Max}(t)} \tag{22}$$

$\vec{a}$ is a vector that linearly varies from 0 to 2, increasing over the iteration process. Additionally, $\vec{r}_1$ and $\vec{r}_2$ are random vectors ranging between 0 and 1. While searching for a solution, the ω wolves update their position in comparison to the optimal solutions (α, β, and δ) as follows (Mohammadi et al., 2020):

$$\vec{X}_1 = \vec{X}_a - \vec{A}_1 \times \left|\vec{C}_1 \times \vec{X}_a - \vec{X}\right| \tag{23}$$

$$\vec{X}_2 = \vec{X}_\beta - \vec{A}_2 \times \left|\vec{C}_2 \times \vec{X}_\beta - \vec{X}\right| \tag{24}$$

$$\vec{X}_3 = \vec{X}_\delta - \vec{A}_3 \times \left|\vec{C}_3 \times \vec{X}_\delta - \vec{X}\right| \tag{25}$$

$$\vec{X}(t+1) = \frac{\vec{X}_1 + \vec{X}_2 + \vec{X}_3}{3} \tag{26}$$

The TR optimization algorithm iteratively minimizes the objective function using a quadratic approximation. The quadratic model approximating the objective function at iteration point x_k is derived from the Taylor series expansion of f around x_k as follows (Nocedal & Wrights, 1999):

$$M\left(\Delta x^k\right) = f\left(x^k\right) + \nabla f\left(x^k\right)\Delta x + \frac{1}{2}\left(\Delta x^k\right)^T B\left(x^k\right)\left(\Delta x^k\right) \tag{27}$$

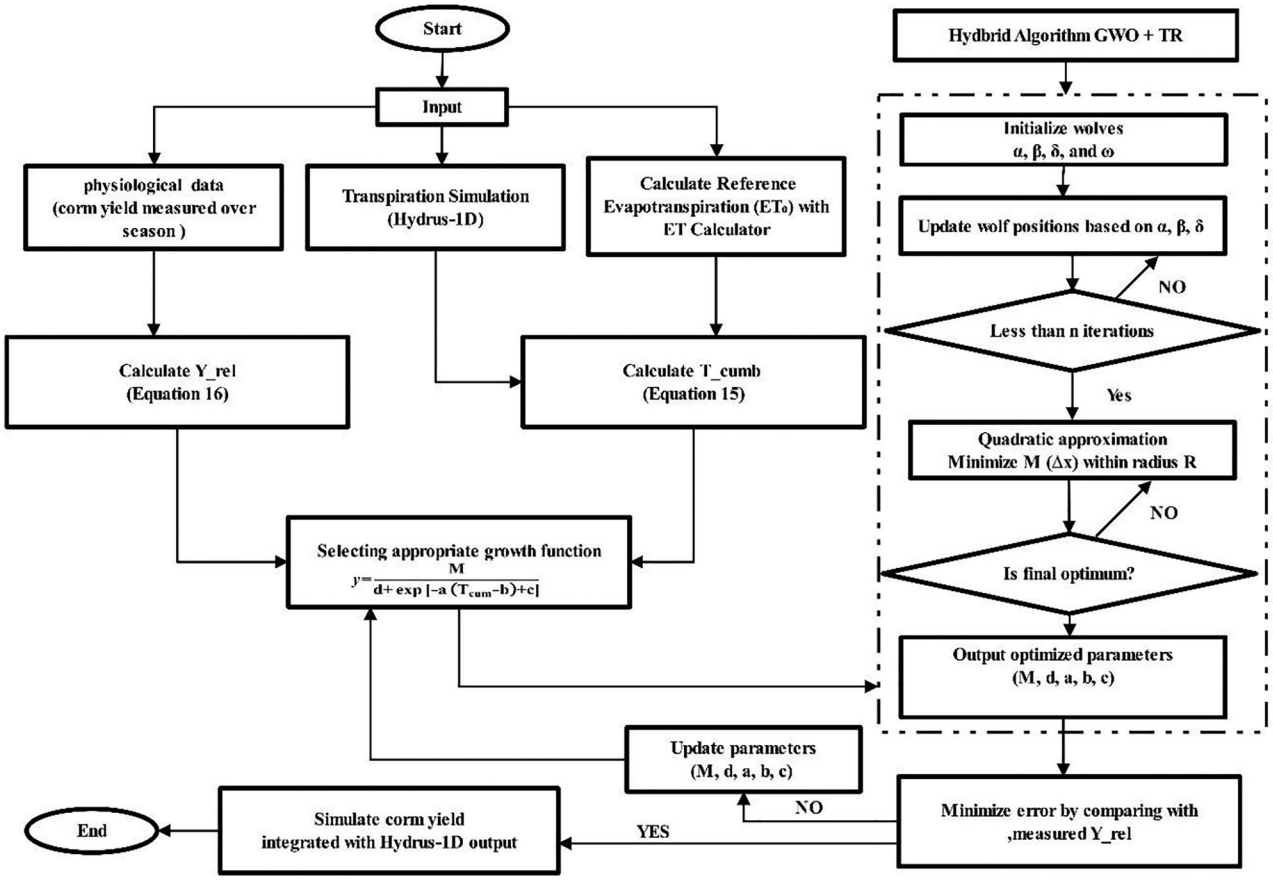

FIGURE 4 Flowchart of the saffron corm yield module and its calibration using the hybrid grey wolf optimizer–trust region (GWO–TR) algorithm.

where $B(x)$ is a symmetric matrix approximating the Hessian of the objective function, $\nabla f(x)$ is the objective function's gradient vector, and Δx is the step size. In the subsequent step, the TR algorithm determines the position of the minimizer of the quadratic approximation within a circular area of radius R by utilizing the constrained optimization as follows:

$$\min M\left(\Delta x^k\right) s.t \Delta x^k \leq R \tag{28}$$

Figure 4 illustrates the linkage between Hydrus-1D and the saffron corm yield module, as well as the hybrid GWO–TR optimization used for calibration.

2.5 | Climate change impact on saffron corm yield

The CMIP6 model data serve as a cornerstone of the Sixth Assessment Report by the Intergovernmental Panel on Climate Change (IPCC). These datasets were developed to address key scientific questions posed in the IPCC reports, enhance understanding of the climate system, and estimate future climate change conditions along with their associated uncertainties. They also provide essential inputs for climate adaptation strategies, test climate predictability, assess model performance in forecasting future decades, and evaluate the accuracy of models in simulating historical climate data. In this phase, multi-model climate projections are refined or updated based on varying scenarios of future greenhouse gas emissions and human-induced land use changes. Climate forecast data are generated by running the model along two main pathways, one of which is the Shared Socioeconomic Pathway (SSP). This pathway explores global trends in population growth, GDP, income distribution, and patterns of societal development. By incorporating various assumptions about regional economic growth, population dynamics, energy consumption, resource availability, and land use over the 21st century, the SSP scenarios project future greenhouse gas emissions and land use changes under different levels of global radiative forcing. These scenarios outline alternative trajectories for climate forcing, typically covering the period from 2006 to 2100 (O'Neill et al., 2016). In this study, the most recent and comprehensive data from three climate models—based on the coupled interactions between the atmosphere, ocean, and land (AOGCM)—were extracted from the CMIP6 series. After a screening process, three models were

TABLE 1 Coupled Model Intercomparison Project Phase 6 (CMIP6) model characteristics used in this study.

Model	Institution	Spatial resolution	Country
MRI-ESM2.0	Meteorological Research Institute, Japan	1.125° × 1.125°	Japan
ACCESS-CM-2	Commonwealth Scientific and Industrial Organisation (CSIRO), Australia, and Bureau of Meteorology (BOM), Australia	1.250° × 1.875°	Australia
MIROC6	National Institute for Environmental Studies, University of Tokyo	1.4° × 1.4°	Tokyo

selected: Japan's MRI-ESM2-0, Australia's ACCESS-CM2, and Japan's MIROC6. These models were chosen based on their availability of complete historical data and future climate scenarios (SSP1-2.6 [optimistic], SSP2-4.5 [intermediate], and SSP5-8.5 [pessimistic]) for key variables such as precipitation, daily maximum temperature, and daily minimum temperature. The specifications of each model are detailed in Table 1. To validate the models, their output was compared with observed data from the Mashhad synoptic station using statistical indicators. The analysis focused on a common 25-year period from 1989 to 2014. First, the model's raw historical data were trimmed to match this timeframe. Then, daily precipitation, as well as minimum and maximum temperature data from the three climate models, was downscaled to the Mashhad station level—that is, bias-corrected—using two statistical methods: linear scaling (LS) and distribution mapping (DM). The LS method is a widely used bias correction approach for adjusting precipitation and temperature outputs from global climate models (GCMs) (Maraun et al., 2010). In the DM approach, the distribution of the simulated GCM data is adjusted to match the distribution of the observed data. The DM method modifies the mean, standard deviation, and quantiles of the simulated data (Themeßl et al., 2012).

2.6 | Statistical analysis

Statistical analysis, including one-way analysis of variance (ANOVA), was conducted for comparing the three scenarios. The analysis was performed using Python (version 3.11) with the statsmodels library.

2.7 | Model evaluation

This study utilized the root mean square error (RMSE), Pearson correlation coefficient (r), and Nash–Sutcliffe efficiency (NSE) to assess the outcomes of the simulations by Hydrus-1D. The best GCM model and the best downscaling method were selected using RMSE, mean absolute error (MAE), bias, R-squared (R^2), concordance correlation coefficient (CCC), Kendall correlation coefficient (τ), Bayesian information criterion (BIC), and corrected Akaike information criterion (AICc).

$$r = \frac{\sum_{i=1}^{n}(O_i - \bar{O}_i)(P_i - \bar{P}_i)}{\sqrt{\sum_{i=1}^{n}(O_i - \bar{O}_i)^2 \sum_{i=1}^{n}(P_i - \bar{P}_i)^2}} \quad (29)$$

$$\mathrm{RMSE} = \sqrt{\frac{\sum_{i=1}^{n}(P_i - O_i)^2}{n}} \quad (30)$$

$$\mathrm{NSE} = 1 - \frac{\sum_{i=1}^{n}\left(O_i - P_i\right)^2}{\sum_{i=1}^{n}\left(O_i - \bar{O}\right)^2} \quad (31)$$

$$MAE = \frac{\sum_{i=1}^{n}\left|\left(O_i - P_i\right)\right|}{n} \quad (32)$$

$$R^2 = \frac{\left(\sum_{i=1}^{n}(O_i - \bar{O}_i)(P_i - \bar{P}_i)\right)^2}{\sum_{i=1}^{n}(O_i - \bar{O}_i)^2 \sum_{i=1}^{n}(P_i - \bar{P}_i)^2} \quad (33)$$

$$\mathrm{Bias} = \frac{\sum_{i=1}^{n}\left(O_i - P_i\right)}{n} \quad (34)$$

$$\mathrm{CCC} = \frac{2\rho\sigma_o\sigma_p}{\sigma_o^2 + \sigma_p^2 + \left(\bar{O} - \bar{P}\right)^2} \quad (35)$$

$$\tau = \frac{(C - D)}{\frac{1}{2} \times (n - 1)} \quad (36)$$

$$\mathrm{AICc} = \frac{2k\,(k+1)}{n - k - 1} + \mathrm{AIC},\ \mathrm{AIC} = -2\ln(L) + 2k \quad (37)$$

$$\mathrm{BIC} = -2\ln L + k\ln(n) \quad (38)$$

In the given context, O_i is the measured value, $\bar{O}_i$ is the mean of measured values, P_i denotes the computed value, $\bar{P}_i$ is the mean of computed values, and n is the total number of observations. ρ represents the Pearson correlation coefficient between the measured and simulated values, while σ_o and σ_p denote the variances of the measured and simulated values, respectively. C and D correspond to the numbers of concordant and discordant pairs. k is the number of model parameters, and L is the likelihood function of the model.

TABLE 2 Initial values of Physicochemical and thermal soil properties.

Type	Parameter	Consistent for all depths	Description
Soil hydraulic parameters of experimental site	θ_r (m^3 m^{-3})	0.078	RETC default
	Alpha	0.036	
	n	1.56	
Salt transport parameters	Longitudinal dispersivity (cm)	10	Hydrus-1D default
	Adsorption isotherm coefficient (g^{-1} cm^3)	0	
	Thermal dispersivity (cm)	5	
Soil thermal parameters	b_1 (g cm s^{-3} °C)	1.56E + 016	Hydrus-1D default
	b_2 (g cm s^{-3} °C)	2.53E + 016	
	b_3 (g cm s^{-3} °C)	9.89E + 016	

TABLE 3 Physicochemical and thermal soil properties required for Hydrus-1D.

		Depth				
Type	Parameter	0–10	10–20	20–30	30–60	Description
Soil hydraulic parameters of experimental site	Texture	Loam	Sandy loam	Sandy clay loam	Sandy loam	Measured
	ρ_b (g cm^{-3})	1.47	1.35	1.57	1.55	Measured
	K_s (mm day^{-1})	49.97	56.18	26.20	94.10	Measured
	θ_s (m^3 m^{-3})	0.4	0.4	0.4	0.45	Measured
	θ_r (m^3 m^{-3})	0.05	0.05	0.067	0.09	Calibrated by RETC
	Alpha	1.175	1.175	1.35	1.3781	Calibrated by RETC
	n	0.01106	0.00637	0.03199	0.00565	Calibrated by RETC
Salt transport Parameters	Longitudinal dispersivity (cm)	0.4	0.0304	23.5	0.077	Calibrated by inverse modeling
	Adsorption isotherm coefficient (g^{-1} cm^3)	2.6	143	83	120	
Soil Thermal Parameters	Thermal dispersivity (cm)	0.15	0.97	4.4	12.7	Calibrated by inverse modeling
	b_1 (g cm s^{-3} °C)	1.19E + 014	1.33E + 016	1.77E + 016	1.61E + 016	
	b_2 (g cm s^{-3} °C)	2.2124E + 016	2.474E + 016	2.579E + 016	2.551E + 016	
	b_3 (g cm s^{-3} °C)	9.088E + 016	9.733E + 016	9.989E + 016	9.922E + 016	

3 | RESULTS AND DISCUSSION

3.1 | Model input parameters

To better illustrate the growing conditions of saffron corm, it is crucial to determine the physicochemical properties of the soil (Amine Ayari et al. 2022). Table 2 presents the initial values of the soil hydraulic parameters (K_s, alpha, and n) used for calibration with the RETC software, together with the assumed initial values of the solute transport and soil thermal parameters. These values were then used as input for the inverse modeling in HYDRUS. The calibrated hydraulic parameters, in addition to the measured K_s and θ_s, as well as the inversely optimized solute transport and soil thermal parameters, are summarized in Table 3t. The root water uptake parameters, derived from Dastranj and Sepaskhah's (2019) research, are presented in Table 4. Figure 5 presents the field-measured values of the LAI, root depth, and canopy cover for the first and second growing seasons. Hydrus-1D utilizes LAI to partition the potential evapotranspiration into potential transpiration and potential evaporation (Wang, Li, Chau, et al., 2021). Whereas the temporal changes are consistent between the 2 years, measured LAI values are larger for the second growing season (3-year-old saffron) as compared to the first growing season (2-year-old saffron). During both seasons, the LAI peaks in winter and declines in spring, which is consistent with Sepaskhah et al. (2013). Sepaskhah et al. (2013) reported that maximum LAI values reached 1.05 during the first growing season and 1.31 during the second growing season. Furthermore, Rezvani-Moghaddam (2020) showed that saffron LAI continues to increase throughout the year, thus explaining the increase in LAI from year to year. The saffron LAI data exhibited follow a nonlinear sigmoidal trend, supporting the findings by Banhangi et al. (2021).

TABLE 4 The root water uptake parameters.

Type	Parameter	Value	Description
Water stress reduction	P0	0 cm	Based on Dastranj and Sepaskhah's (2019) research + calibration
	P0pt	−1 cm	
	P2H	−402.262 cm	
	P2L	−2636.11 cm	
	P3	−90,359.3 cm	
	r2H	1 cm day^{-1}	
	r2L	0.1 cm day^{-1}	
Salinity stress reduction	Threshold	2	
	Slope	0.33	
	C_{max}	10	

3.2 | Calibration

3.2.1 | Soil water content

Figure 6a compares field-measured (0- to 20-cm soil layer) with simulated soil water content throughout the first growing season, resulting in an RMSE value of 0.034 cm^3/cm^3, an NSE equal to 0.79, and a Pearson correlation coefficient (r) of 0.9. These statistics show that Hydrus-1D was successful in simulating soil water content during the first growing season, as indicated by statistical indices (RMSE, NSE, and r). Our values were better than those presented by Zhang et al. (2024), using the Hydrus-1D model. Mirsafi et al. (2016) simulated soil water content in a saffron field with satisfactory accuracy using the AquaCrop model. However, the measurement data available for model calibration were considerably limited, with soil water content measured only once per growing season, in contrast to the present study, which conducted measurements with high temporal resolution. Sepaskhah et al. (2013) also developed a dynamic model for farmers to use in saffron fields. However, despite the model's capability to simulate saffron yield, it failed to accurately simulate soil water content, likely due to insufficient data. This model was later calibrated by Yarami and Sepaskhah (2015) to simulate saffron growth under salinity and different manure levels, but it still tended to either overestimate or underestimate soil water content.

3.2.2 | Salt transport

The soil salinity data collected throughout the first growing season were utilized to calibrate the Hydrus-1D model. Unlike water-driven "tipping bucket" models such as AquaCrop that rely on empirical equations, Hydrus-1D incorporates dispersion, diffusion, and convection. The solute transport equations account for advective-dispersive transport in the liquid phase (Šimůnek et al., 2007). The RMSE, r, and NSE for simulating soil salinity using the Hydrus-1D model were 0.079 dS/m, 0.78, and 0.95, respectively, during the first growing season (Figure 7a). A comparison of the measured and simulated salinity data from the first growing season, along with the statistical indicators, revealed that the Hydrus-1D model effectively captures the details of saline soil dynamics. The simulated soil salinity is in accordance with measurements of Yarami and Sepaskhah (2015), who reported that the soil salinity was between 0.62 and 1.64 dS/m. Hydrus-1D successfully simulates soil salinity up to a depth of 20 cm throughout the growing season. Following the calibration of the Hydrus-1D model by Kanzari et al. (2018) for simulating soil salinity under various field conditions, the model was shown to predict soil salinity levels with a high degree of accuracy.

3.2.3 | Heat transfer

Soil temperatures were calibrated for the Hydrus-1D model in Figure 8a by using the first growing season data. For the calibration period, the comparison between measured and simulated soil temperatures resulted in an RMSE of 1.43°C, an NSE of 0.93, and an r value of 0.97. The statistical analysis comparing observation data with simulations generated by the Hydrus-1D model indicates that the model can accurately predict temperatures for the first growing season of saffron crops.

3.3 | Validation

3.3.1 | Soil water content

The calibrated model was further validated using the soil water content observations from the second growing season

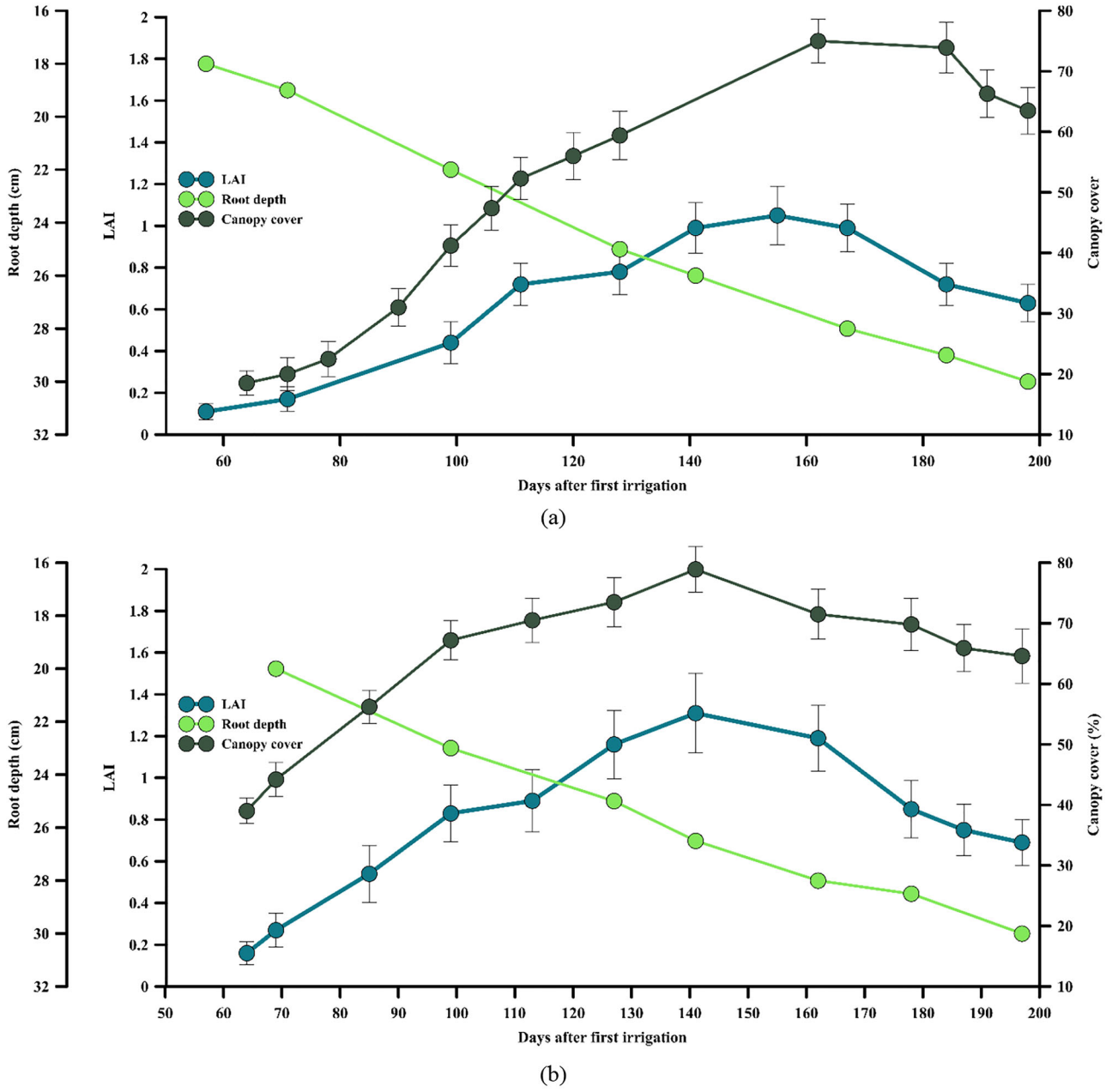

FIGURE 5 Measured rooting depth, leaf area index (LAI), and canopy cover values during the first (2021–2022) and second growing season (2022–2023).

of 3-year saffron. As shown in Figure 6b, the statistical comparison between observed and modeled values was similar to the calibration for the first season, with values for RMSE, *r*, and NSE equal to 0.027 cm^3/cm^3, 0.87, and 0.63, respectively. Hydrus-1D simulations were able to compute both the sudden increases in soil water content after irrigation as well as its gradual decreases in the drying stage for both the calibration and validation phases, similar to the research findings of Ngam et al. (2017). Also in their work, it was shown that the Hydrus-1D model was able to accurately simulate soil water content when compared with TDR 350 measured values. The findings suggest that the Hydrus-1D model simulates soil water content with acceptable and similar accuracies.

3.3.2 | Salt transport

The model, calibrated with data from the first growing season, was validated using data from the second growing season. The statistical indicators for soil salinity simulation in the second growing season included an RMSE of 0.19 dS/m, an NSE of 0.22, and an *r* value of −0.52 (Figure 7b). These statistical indicators showed that the Hydrus-1D model was less

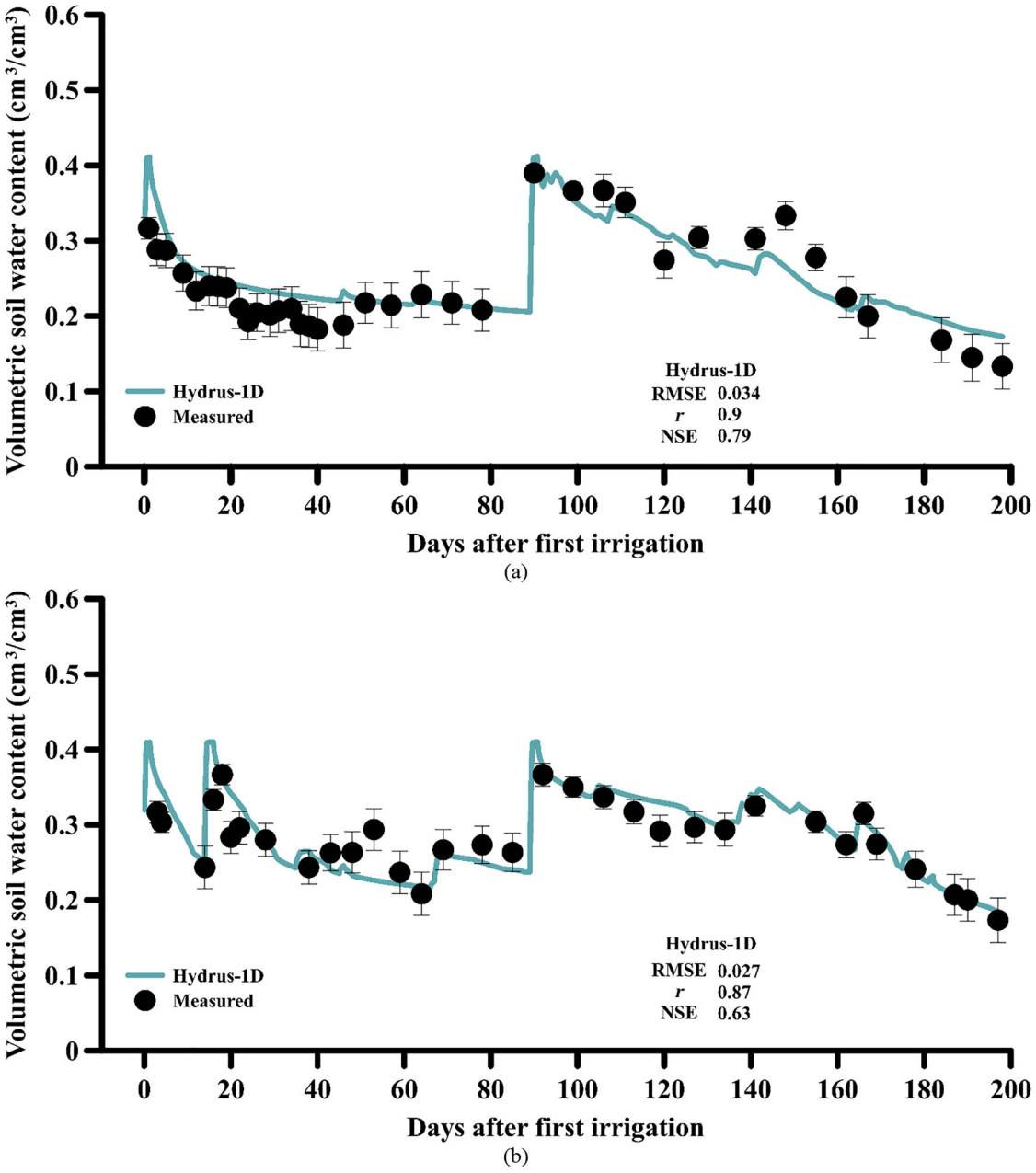

FIGURE 6 Comparison of simulated with measured soil water content values for (a) the calibration year (2021–2022) and (b) the validation year (2022–2023). NSE, Nash–Sutcliffe efficiency; RMSE, root mean square error.

accurate in estimating soil salinity during the second season (3-year saffron) compared to the first. Its performance in simulating salinity, particularly after the second irrigation, was notably poor. As previously noted, the simulation of soil salinity in the second-year Hydrus-1D model lacked the desired accuracy. One potential reason for this discrepancy is the increased frequency of irrigation in the second growing season compared to the first. During the second growing season, additional irrigation was conducted, which may have intensified the fluctuations in soil salinity simulation throughout the growing season. Another possible reason for the deviation between the simulated and measured salinity values in the second growing season could be that the model was calibrated using data from the first growing season only.

3.3.3 | Heat transfer

The model calibrated for soil temperature simulation in the first growing season was validated with data from the second growing season. For the validation period, RMSE was 1.54°C, NSE was 0.94, and r value was 0.99 (Figure 8b). It effectively simulates soil temperature conditions up to a depth of 20 cm for saffron crops during growing seasons with

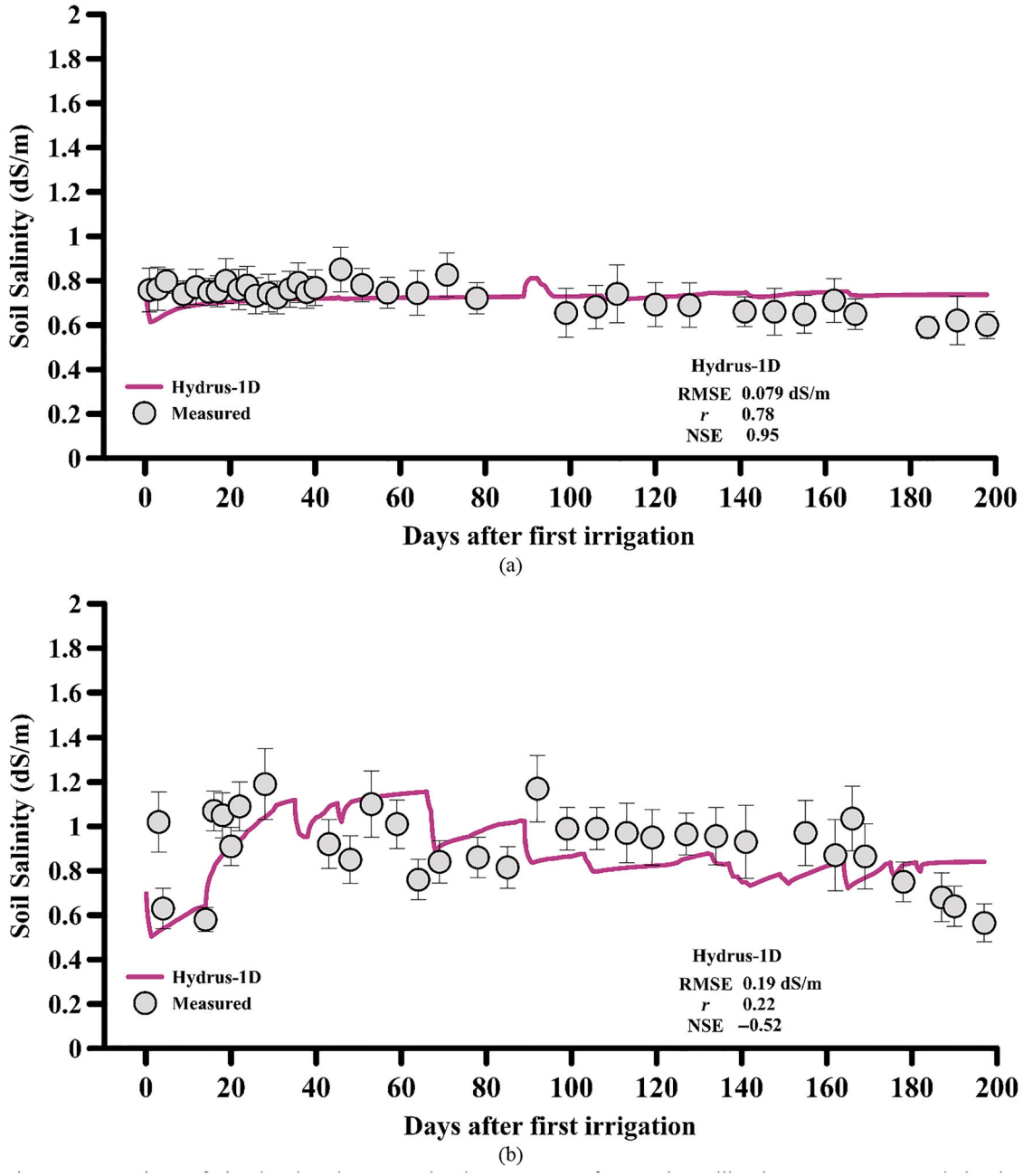

FIGURE 7 Comparison of simulated and measured solute transport for (a) the calibration (2021–2022) and (b) the validation year (2022–2023). NSE, Nash–Sutcliffe efficiency; RMSE, root mean square error.

varying temperature extremes. Limited studies have shown the effectiveness of the Hydrus model for simulating field soil temperature. Such a study by Deb et al. (2011) indicated that although the model was able to simulate the general trend of observed soil temperature, model temperatures were significantly underestimated, as caused by lacking accurate soil heat parameters. Our study showed remarkably accurate soil temperature simulation results, likely caused by applying the soil thermal parameters by Chung and Horton (1987), specific to clay loam soil (Kassaye et al., 2021). Other studies such as by Kodešová et al. (2014) and Yadav et al. (2020) also confirmed that Hydrus1D can accurately simulate soil temperature regimes, albeit for relatively short time scales. Our study shows excellent results for long-term seasonal time scales but is limited to the shallow root zone only. Akbari et al. (2024) investigated the impact of freezing and heat stress on saffron corms across six primary saffron-growing regions in Iran, concluding that corms exhibit greater sensitivity to freezing than to heat stress. In their study, only air temperature was involved due to the limitations of the AquaCrop model, which could not simulate soil temperature, and its influence on corm production remained uncertain. While air

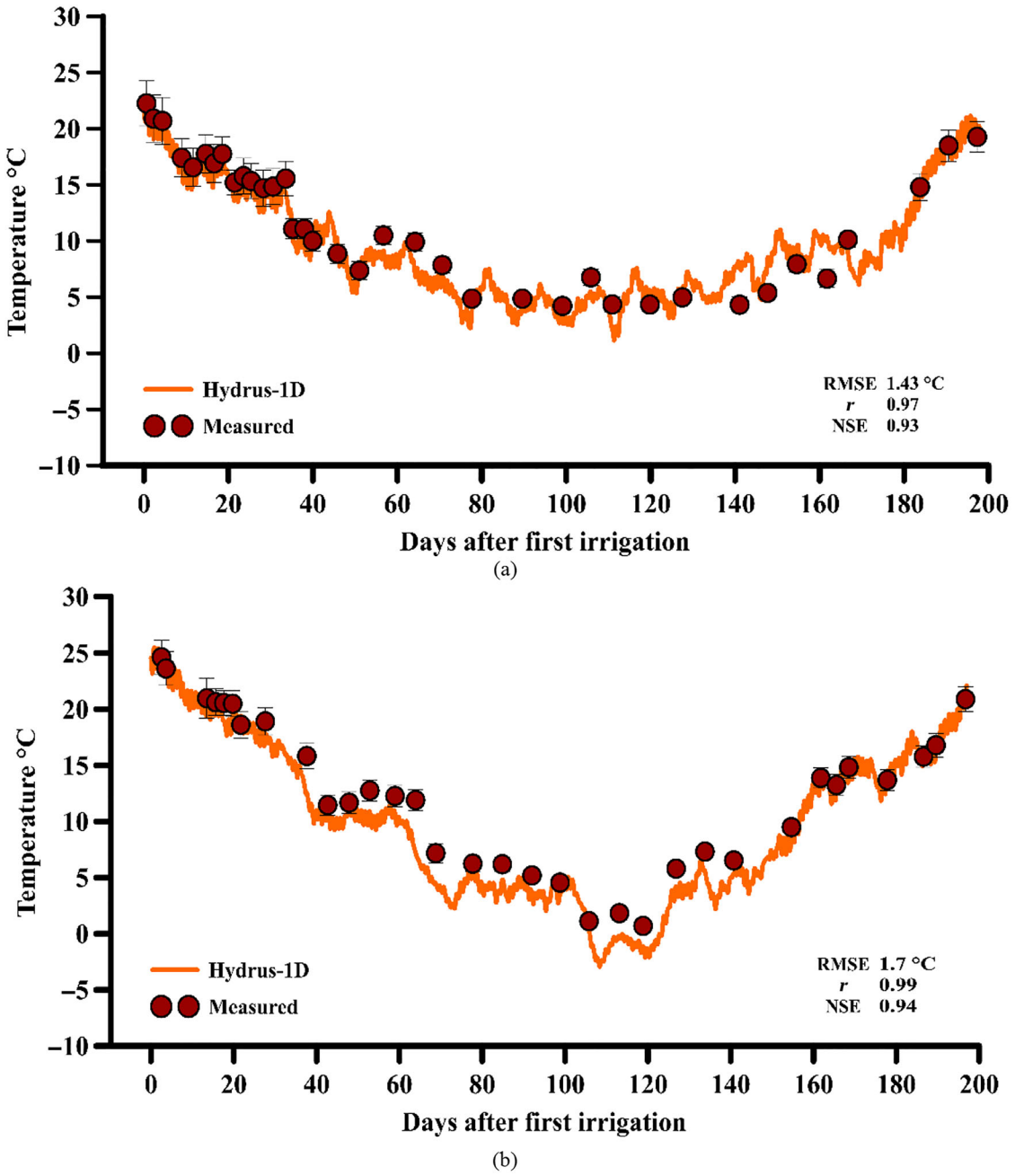

FIGURE 8 Comparison of simulated soil temperature by Hydrus-1D with measured data for (a) the calibration (2021–2022) and (b) the validation year (2022–2023). NSE, Nash–Sutcliffe efficiency; RMSE, root mean square error.

temperature plays a key role in initiating saffron flowering (Renau-Morata et al., 2021), soil temperature is more significant for the development of saffron corms (Sepaskhah & Kamgar-Haghighi, 2009), which begins after the flowering stage ends. The present findings are consistent with Khaliq et al. (2024), who reported that both soil texture and temperature significantly affect floral, stigma, corm, and quality traits of saffron. In their study, optimal floral and stigma yields were observed in loam-textured soils at around 26˚C, emphasizing the role of moderate soil temperature in enhancing saffron performance. The close alignment between our modeling results and their experimental observations highlights the critical importance of soil temperature in saffron cultivation and validates the use of Hydrus-1D as a predictive tool for assessing crop yield under different climatic and soil conditions. So far, no research has simulated soil temperature in saffron fields with high temporal resolution. To address this gap, this study employs the Hydrus-1D model to simulate soil temperature for saffron. Saffron requires a drop in air temperature to start flowering. During this phase, the flowers are exposed to the air, making air temperature more influential than soil temperature. However, during the corm production

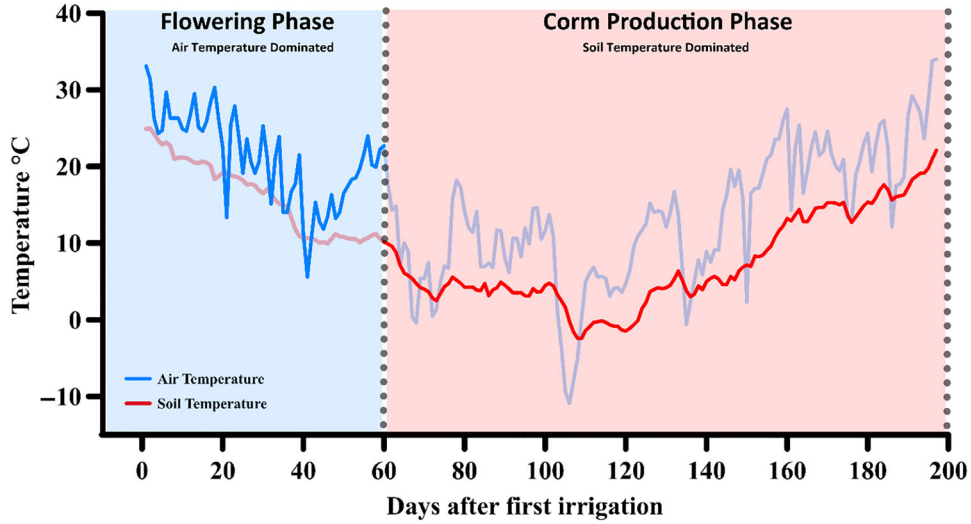

FIGURE 9 Dominancy of air and soil temperature and its influence on the flowering phase and corm production phase.

period, the corms—located about 20 cm deep in the soil—are in direct contact with the soil, so soil temperature becomes the more critical factor. Therefore, air temperature is the dominant factor during the flowering period, whereas soil temperature becomes the dominant factor during the corm production phase, which starts after flowering ends. Figure 9 distinctly shows the disparity between soil and air temperatures during the corm production phase, highlighting the necessity of simulating soil temperature to achieve more precise corm yield prediction at the end of the growing season. The current study demonstrates that Hydrus-1D, when calibrated with high-resolution field data, can effectively reproduce the thermal regime of saffron fields. This provides a more reliable framework for predicting crop responses under changing climatic conditions and distinguishes our approach from earlier studies that either ignored or simplified soil temperature processes.

3.3.4 | Corm yield calculated with new module

With the hybrid GWO–TR algorithm method, the data from the first growing season were fitted to Equation (17), as outlined in Section 2. The equation coefficients and error indicators are shown in Table 5. Thus, corm yield for the first growing season was simulated using Equation (17), based on transpiration calculated by the Hydrus-1D model (Figure 10). It was determined that the module simulated corm yield with RMSE of 0.16 tonne/ha, NSE of 0.99, and r value of 86. The corm weight simulated by the module for the first growing season is consistent with the values measured by Karra et al. (2017) and Koocheki et al. (2022). As shown in Figure 11, corm yield values for the second growing season were simulated using Equation (17) and the coefficients derived from the first growing season. Saffron corm yield was simulated with RMSE of 0.4 tonne/ha, NSE of 0.97, and r of 0.89. Based on statistical indicators, the module demonstrated acceptable accuracy in simulating corm yield during the second growing season.

TABLE 5 Coefficients of new module equation with error indices.

Coefficients				
m	***d***	***a***	***b***	***c***
0.47734	−0.97548	0.003295	55.4496	−2.095
Error indices				
	Phase	**RMSE**	**MAE**	**NSE**
	Calibration	0.0738	0.0508	0.9994
	Validation	0.121	0.0676	0.9981

Abbreviations: MAE, mean absolute error; NSE, Nash–Sutcliffe efficiency; RMSE, root mean square error.

Despite the increase in soil salinity in the second year, the yield was higher compared to the first year. Since saffron is a perennial crop and its growth continues from year to year, producing a more extensive root network each year (Koocheki & Seyyedi, 2015), it is therefore expected that the yield in the second year through the corms, when the corms were 3 years old, would be higher than in the first year, when the corms were 2 years old.

3.3.5 | Climate change impact on saffron corm yield on near future

Table 6 shows the validation results of climate models, based on eight statistical indices—bias, MAE, RMSE, R^2, τ (Kendall correlation coefficient), CCC, BIC, and AICc—calculated for monthly aggregated data to facilitate easier

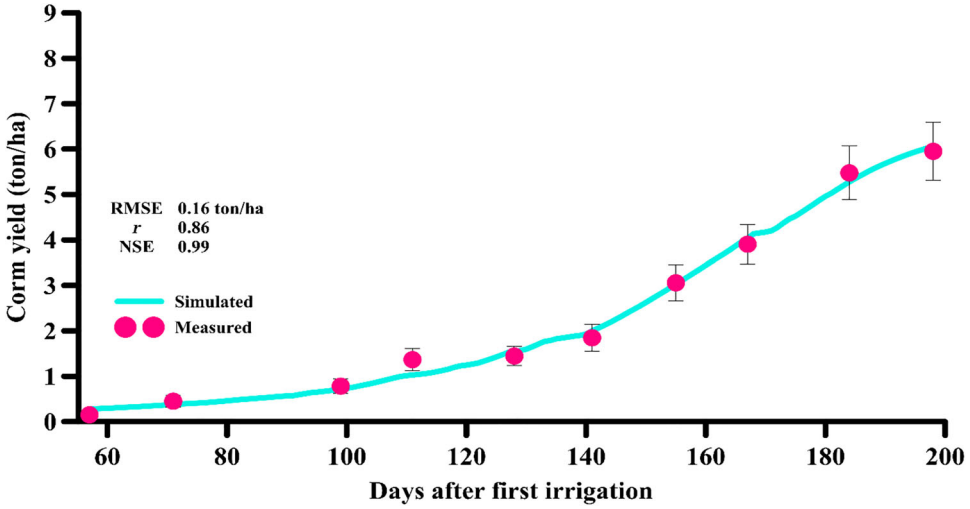

FIGURE 10 Comparison of measured and simulated corm yield with the new module at the first growing season (2021–2022). NSE, Nash–Sutcliffe efficiency; RMSE, root mean square error.

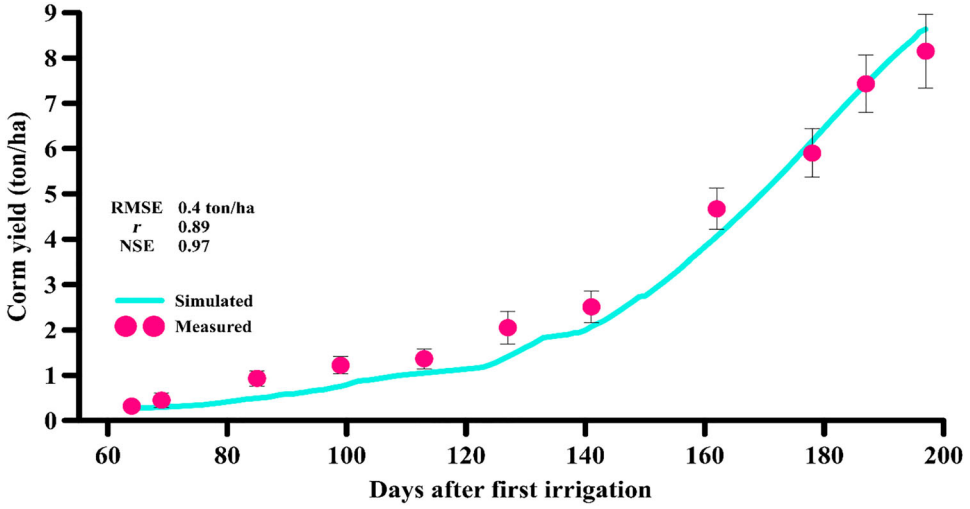

FIGURE 11 Comparison of measured and simulated corm yield with the new module at the second growing season (2022–2023). NSE, Nash–Sutcliffe efficiency; RMSE, root mean square error.

comparison, and also includes the results for the raw, unprocessed data, indicating improvement in performance during the downscaling process. This suggests that applying bias correction techniques enhances the accuracy of downscaled precipitation and minimum/maximum temperature data derived from large-scale atmospheric–oceanic general circulation models. Among the evaluated models, MRI-ESM2-0 outperforms ACCESS-CM2 and MIROC6 for daily precipitation and maximum temperature, while ACCESS-CM2 shows better performance for minimum temperature data. For future climate projections, LS is recommended for bias correction of precipitation, whereas DM is preferable for correcting minimum and maximum temperature data. Figures 12–14 display the simulated corm yield results using the new Hydrus-1D module under three different scenarios from 2025 to 2050 (near future). For clearer comparison, each figure also includes the corresponding annual values of cumulative transpiration and precipitation. It is important to note that all simulations were performed using the Hydrus-1D model for a 3-year-old saffron crop. Under scenario SSP126, the highest corm yield reached 12.21 tonne/ha in 2037, while the lowest yield was 10.15 tonne/ha in 2048. In scenario SSP245, the maximum corm yield was recorded in 2040 at 12.39 tonne/ha, with the minimum of 10.07 tonne/ha occurring in 2043. For scenario SSP585, the highest corm yield occurred in 2021 at 12.22 tonne/ha, whereas the lowest yield—9.11 tonne/ha—was in 2026. In this study, irrigation scheduling was carried out under real field conditions and was based on the farmer's traditional experience rather than on soil water content monitoring or ET-based methods. It was assumed that

TABLE 6 Coupled Model Intercomparison Project Phase 6 (CMIP6) models calibration evaluation.

Model	Parameter	Downscaling method	Bias	MAE	RMSE	R^2	τ	CCC	BIC	AICc
MRI-ESM2-0	Precipitation	RAW	18.91	25.49	37.76	0.23	0.45	0.37	2277.43	2269.98
		DM	1.51	17.26	27.12	0.22	0.48	0.46	2070.81	2063.36
		LS	0.02	13.35	20.18	0.34	0.51	0.57	1886.34	1878.89
	Maximum temperature	RAW	−2.62	3.65	4.7	0.91	0.81	0.91	977.09	969.64
		DM	0	2.2	2.95	0.91	0.8	0.95	686.7	679.25
		LS	0	2.32	3.06	0.9	0.79	0.95	710.21	702.77
	Minimum temperature	RAW	−0.56	1.9	2.46	0.91	0.79	0.95	573.59	566.15
		DM	0	1.73	2.34	0.92	0.81	0.95	542.42	534.98
		LS	0	1.69	2.26	0.92	0.81	0.96	521.53	514.08
ACCESS-CM-2	Precipitation	RAW	7.5	18.93	30.54	0.19	0.45	0.41	2144.94	2137.49
		DM	1.16	17.61	27.71	0.17	0.41	0.4	2084.28	2076.84
		LS	0.03	15.03	23.36	0.23	0.45	0.48	1977.82	1970.37
	Maximum temperature	RAW	−3.83	4.25	5.16	0.89	0.77	0.88	1034.86	1027.41
		DM	0	2.33	3.13	0.9	0.79	0.95	724.22	716.77
		LS	0	2.49	3.31	0.89	0.77	0.94	757.49	750.04
	Minimum temperature	RAW	−0.04	1.93	2.54	0.91	0.8	0.95	592.39	584.94
		DM	0.01	1.65	2.19	0.93	0.82	0.96	500.15	492.71
		LS	0.01	1.83	2.41	0.91	0.81	0.95	559.12	551.67
MIROC6	Precipitation	RAW	9.88	20.97	31.92	0.2	0.43	0.4	2172.5	2165.05
		DM	1.58	18.76	30.58	0.13	0.39	0.35	2145.71	2138.26
		LS	0.02	15.11	22.95	0.23	0.44	0.48	1966.55	1959.11
	Maximum temperature	RAW	7.89	8.18	9.83	0.91	0.8	0.73	1437.61	1430.16
		DM	0	2.32	3.1	0.9	0.79	0.95	716.54	709.09
		LS	0	2.44	3.16	0.9	0.78	0.94	729.83	722.38
	Minimum temperature	RAW	7.33	7.35	8.12	0.91	0.81	0.7	1318.22	1310.77
		DM	0	1.64	2.26	0.92	0.82	0.96	520.15	512.7
		LS	0	1.68	2.27	0.92	0.81	0.96	522.3	514.85

Abbreviations: AICc, corrected Akaike information criterion; BIC, Bayesian information criterion; CCC, concordance correlation coefficient; DM, distribution mapping; LS, linear scaling; MAE, mean absolute error; RMSE, root mean square error.

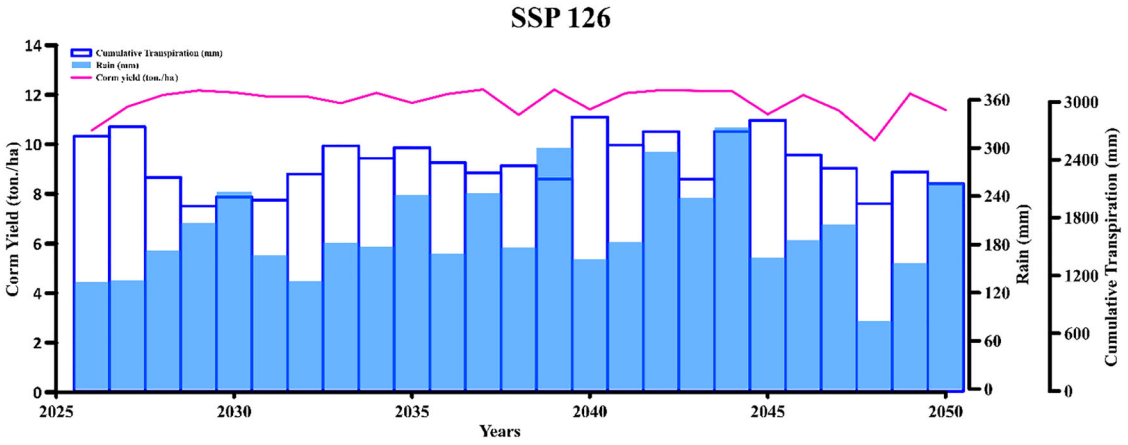

FIGURE 12 Variations of corm yield, rainfall, and cumulative evapotranspiration from 2025 to 2050 under the SSP126 (where SSP stands for Shared Socioeconomic Pathways) scenario.

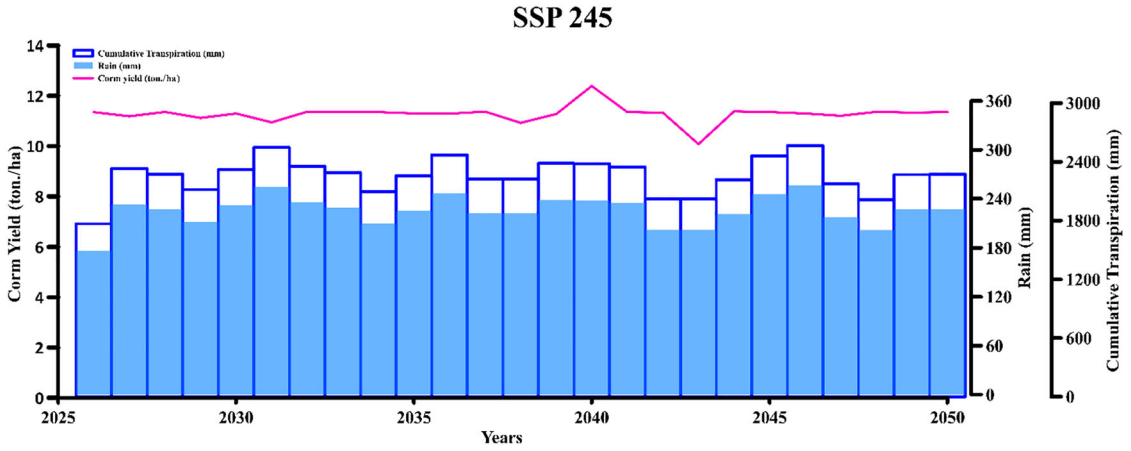

FIGURE 13 Variations of corm yield, rainfall, and cumulative evapotranspiration from 2025 to 2050 under the SSP245 (where SSP stands for Shared Socioeconomic Pathways) scenario.

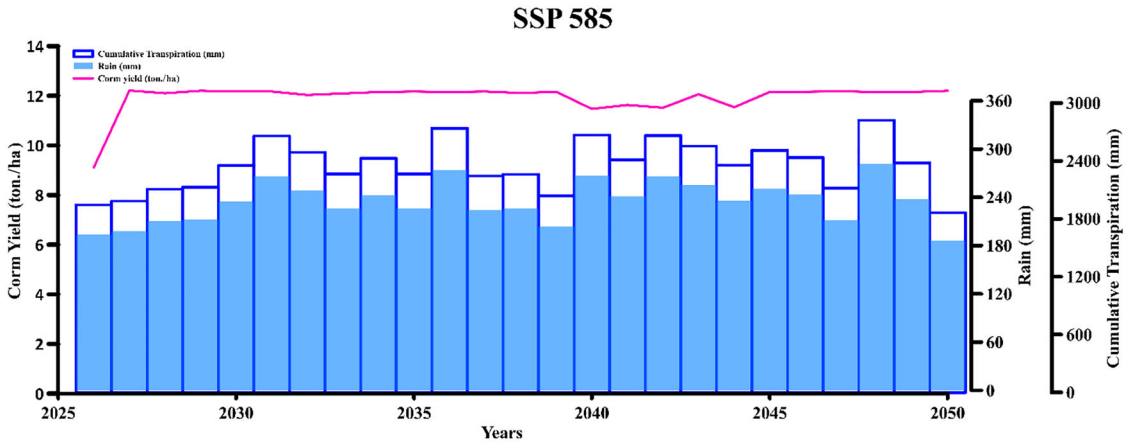

FIGURE 14 Variations of corm yield, rainfall, and cumulative evapotranspiration from 2025 to 2050 under the SSP585 (where SSP stands for Shared Socioeconomic Pathways) scenario.

the same practice would be maintained in the near future; therefore, the irrigation regime applied in the experimental period represents the expected management conditions under future scenarios.

While examination of the results suggests small fluctuations between scenarios, statistical validation was performed to support these observations. A one-way ANOVA was conducted on the 25-year dataset, which indicated statistically significant differences among the scenarios ($F = 10.31$, $p < 0.001$). Despite the statistical significance, the magnitude of the yield differences is relatively small, ranging roughly between 10 and 12.4 tonne/ha across scenarios. This shows that saffron corm yield in Mashhad is likely to remain largely unaffected by climate change in the near future. For instance, under SSP585, the maximum annual yield reached 12.22 tonne/ha, while the minimum was 9.11 tonne/ha. Similarly, SSP245 and SSP126 showed comparable ranges, confirming that the overall yield remains stable. Cumulative transpiration and precipitation values are also presented in Figures 12–14.

According to CMIP6 projections, rainfall in Mashhad is expected to slightly increase in the near future, which may further help maintain yield stability. These results reinforce that saffron remains a suitable crop for cultivation under projected climate scenarios, supporting its resilience and reliability for near-future agricultural planning. This projected increase in rainfall for Mashhad aligns with the findings of Asgharzadeh et al. (2024). Climate plays a crucial role in determining saffron yield and significantly restricts its cultivation in many parts of the world (Pirasteh-Anosheh et al., 2023). Hence, the geographical location—encompassing elements such as altitude and latitude—plays a critical role in shaping the environmental conditions that directly impact saffron yield (Zamani et al., 2022). Since ancient times, the cities of Qayen, Birjand, Gonabad, and Ferdows, located between latitudes 32° and 34°, have served as the primary centers for extensive saffron cultivation in Iran, and the climate in these regions is considered well-suited for growing saffron (Ghorbani & Koocheki, 2017). However, climate change has cast doubt

on the long-term sustainability of these regions for saffron cultivation. Recent studies have shown that moving saffron cultivation to cooler regions could be an effective strategy for maintaining its economic yield (Askari-Khorasgani et al., 2019). Therefore, planting saffron at higher latitudes could be one potential solution to mitigate the negative impacts of climate change on the saffron crop. Mashhad is located at a higher latitude than the traditional saffron-growing cities mentioned earlier, yet it still offers suitable conditions for saffron cultivation. Findings from the present study indicate that Mashhad could serve as a viable region for saffron cultivation in the future, with climate change unlikely to significantly impact saffron corm yield at least until 2050.

However, these projections are subject to certain limitations, as the yield module was simplified and based mainly on cumulative transpiration under static soil properties and traditional irrigation management. Incorporating dynamic soil–crop interactions, alternative irrigation strategies, and multiple GCM ensembles in future work would help refine these results.

4 | CONCLUSION

In this study, the Hydrus-1D model was calibrated and validated using high-resolution measured data to simulate soil water content, salinity, and temperature in a saffron-cultivated field. The results demonstrated that the Hydrus-1D model can simulate soil water content and soil temperature for 2- (calibration) and 3-year-old (validation) saffron crops with high accuracy. However, the model achieved acceptable accuracy in simulating soil salinity only for 2-year-old saffron. Recognizing that soil temperature plays a more critical role in corm development than air temperature, this served as the rationale behind employing the Hydrus-1D model to simulate soil temperature dynamics. On the other hand, the Hydrus-1D model has limitations, as it cannot simulate aboveground crop organs and is restricted to model actual evaporation and transpiration. Therefore, in this study, a novel and simple crop yield simulation module was implemented within the Hydrus-1D model using hybrid GWO and TR algorithms. This module was used to assess the impact of climate change on saffron corm yield. The new module, combined with models from CMIP6, was used to evaluate the impact of climate change on saffron corm production in Mashhad for the near future (2025–2050): MRI-ESM2-0, ACCESS-CM2, and MIROC6. To achieve this, the three models—MRI-ESM2-0, ACCESS-CM2, and MIROC6—were first validated by comparing historical and observational data using two downscaling methods. Based on these evaluations, data from model MRI-ESM2-0 were selected as the most accurate, using the LS method for precipitation and the DM method for maximum temperatures. Also, ACCESS-CM2 showed better performance for minimum temperature data using the DM method. Using the selected data, corm production was then simulated under three scenarios including SSP126, SSP245, and SSP585 for the period 2025–2050. The simulation results showed that, across all three scenarios, saffron corm yield in Mashhad will remain largely unaffected by climate change in the near future. This indicates that saffron, historically grown in regions at lower latitudes than Mashhad, could become a profitable crop in higher latitude regions like Mashhad in the future. These findings confirm that saffron is a resilient crop under projected near-future climate conditions in Mashhad, and its yield is not expected to experience substantial reductions. The demonstrated stability of saffron yields highlights its potential as a strategic crop for climate change adaptation in water-scarce regions of northeastern Iran. Policymakers can encourage its cultivation to enhance agricultural sustainability under limited water resources.

This study employed a simplified yield module based on cumulative transpiration and assumed static soil properties and traditional irrigation management. Moreover, potential biotic and abiotic stresses were not explicitly included. Moreover, work should incorporate dynamic soil and crop processes, alternative irrigation strategies, and multiple GCM ensembles to refine the projections.

AUTHOR CONTRIBUTIONS

Amir Akbari: Investigation; methodology; software; validation; writing—original draft. **Ali Naghi Ziaei**: Investigation; methodology; software; validation; writing—original draft. **Seyed Mohammadreza Naghedifar**: Methodology; software; writing—review and editing. **Jan W. Hopmans**: Writing—review and editing. **Jamile Gholipour**: Data curation.

ACKNOWLEDGMENTS

This research has been financially supported by the Saffron Institute, University of Torbat Heydarieh. Torbat Heydarieh, Iran.The grant number was 179755.

CONFLICT OF INTEREST STATEMENT

The authors declare no conflicts of interest.

ORCID

Amir Akbari https://orcid.org/0000-0003-2514-2892
Ali Naghi Ziaei https://orcid.org/0000-0001-6477-5719
Seyed Mohammadreza Naghedifar https://orcid.org/0000-0003-4903-9507
Jan W. Hopmans https://orcid.org/0000-0002-4807-2172
Jamile Gholipour https://orcid.org/0009-0008-5265-1004

REFERENCES

Abbasi, M. R., & Sepaskhah, A. R. (2023). Nitrogen leaching and groundwater N contamination risk in saffron/wheat intercropping

under different irrigation and soil fertilizers regimes. *Scientific Reports*, *13*(1), Article 6587. https://doi.org/10.1038/s41598-023-33817-5

Abedinpour, M., Sarangi, A., Rajput, T. B. S., Singh, M., Pathak, H., & Ahmad, T. (2012). Performance evaluation of AquaCrop model for maize crop in a semi-arid environment. *Agricultural Water Management*, *110*, 55–66. https://doi.org/10.1016/j.agwat.2012.04.001

Akbari, A., Ziaei, A. N., Naghedifar, S. M., Moghaddam, P. R., & Sharafkhane, M. G. (2024). Simulation of saffron growth using AquaCrop model with high-resolution measured data. *Scientia Horticulturae*, *324*, Article 112569. https://doi.org/10.1016/j.scienta.2023.112569

Akramiani, S., Afsahi, M. M., & Akhavan, H. R. (2024). Optimization of encapsulation and spouted bed drying of saffron petal extract and evaluation of its thermal stability in natural pomegranate juice. *Journal of Food Measurement and Characterization*, *18*(5), 1–11.

Amine Ayari, M., Denis, M. P., Landry, G. A., & Lapointe, L. (2022). Cultivation of Saffron (*Crocus sativus* L.) in cold climates. *Canadian Journal of Plant Science*, *102*(3), 608–627. https://doi.org/10.1139/cjps-2021-0053

Asgharzadeh, A., Gobadijanbaz, G., Motevalli, S., Taherian, M., & Kouhi, M. (2024). Examining the climate extreme indices of temperature and precipitation under the conditions of climate change in Razavi Khorasan province. *Journal of Climate Research*, *1403*(57), 63–78.

Askari-Khorasgani, O., & Pessarakli, M. (2019). Shifting saffron (*Crocus sativus* L.) culture from traditional farmland to controlled environment (greenhouse) condition to avoid the negative impact of climate changes and increase its productivity. *Journal of Plant Nutrition*, *42*(19), 2642–2665.

Bali, N., & Singla, A. (2022). Emerging trends in machine learning to predict crop yield and study its influential factors: A survey. *Archives of Computational Methods in Engineering*, *29*(1), 95–112. https://doi.org/10.1007/s11831-021-09569-8

Banhangi, F. M., Moghaddam, P. R., Asadi, G. A., & Khorramdel, S. (2021). Do corm seeding rate and planting depth influence growth indicators of saffron (*Crocus sativus* L.)?. *Industrial Crops and Products*, *174*, Article 114145. https://doi.org/10.1016/j.indcrop.2021.114145

Bazrafshan, O., Etedali, H. R., Moshizi, Z. G. N., & Shamili, M. (2019). Virtual water trade and water footprint accounting of saffron production in Iran. *Agricultural Water Management*, *213*, 368–374. https://doi.org/10.1016/j.agwat.2018.10.034

Bouyoucos, G. J. (1962). Hydrometer method improved for making particle size analyses of soils. *Agronomy Journal*, *54*(5), 464–465. https://doi.org/10.2134/agronj1962.00021962005400050028x

Cardone, L., Castronuovo, D., Perniola, M., Cicco, N., & Candido, V. (2019). Evaluation of corm origin and climatic conditions on saffron (*Crocus sativus* L.) yield and quality. *Journal of the Science of Food and Agriculture*, *99*(13), 5858–5869. https://doi.org/10.1002/jsfa.9860

Chen, S., Mao, X., Barry, D. A., & Yang, J. (2019). Model of crop growth, water flow, and solute transport in layered soil. *Agricultural Water Management*, *221*, 160–174. https://doi.org/10.1016/j.agwat.2019.04.031

Chung, S. O., & Horton, R. (1987). Soil heat and water flow with a partial surface mulch. *Water Resources Research*, *23*(12), 2175–2186. https://doi.org/10.1029/WR023i012p02175

Darvish, H., Ramezan, Y., Khani, M. R., & Kamkari, A. (2022). Effect of low-pressure cold plasma processing on decontamination and quality attributes of saffron (*Crocus sativus* L.). *Food Science & Nutrition*, *10*(6), 2082–2090. https://doi.org/10.1002/fsn3.2824

Dastranj, M., & Sepaskhah, A. R. (2019). Saffron response to irrigation regime, salinity and planting method. *Scientia Horticulturae*, *251*, 215–224. https://doi.org/10.1016/j.scienta.2019.03.027

Deb, S. K., Shukla, M. K., Sharma, P., & Mexal, J. G. (2011). Coupled liquid water, water vapor, and heat transport simulations in an unsaturated zone of a sandy loam field. *Soil Science*, *176*(8), 387–398. https://doi.org/10.1097/SS.0b013e318221f132

De Marsily, G. (1986). *Quantitative hydrogeology*. Academic Press.

De Vries, D. A. (1963). The thermal properties of soils. In R. W. van Wijk (Ed.), *Physics of plant environment* (pp. 210–235). North-Holland Publishing Co.

Feddes, R. A., Kowalik, P. J., & Zaradny, H. (1978). *Simulation of field water use and crop yield*. John Wiley & Sons.

Ghorbani, R., & Koocheki, A. (2017). Sustainable cultivation of saffron in Iran. In *Sustainable agriculture reviews* (pp. 169–203). Springer Nature. https://doi.org/10.1007/978-3-319-58679-3_6

Gresta, F., Avola, G., Lombardo, G. M., Siracusa, L., & Ruberto, G. (2009). Analysis of flowering, stigmas yield and qualitative traits of saffron (*Crocus sativus* L.) as affected by environmental conditions. *Scientia Horticulturae*, *119*(3), 320–324. https://doi.org/10.1016/j.scienta.2008.08.008

Jiménez-Martínez, J., Skaggs, T. H., Van Genuchten, M. T., & Candela, L. (2009). A root zone modelling approach to estimating groundwater recharge from irrigated areas. *Journal of Hydrology*, *367*(1–2), 138–149.

Jones, J. W., Hoogenboom, G., Porter, C. H., Boote, K. J., Batchelor, W. D., Hunt, L. A., Wilkens, P. W., Singh, U., Gijsman, A. J., & Ritchie, J. T. (2003). The DSSAT cropping system model. *European Journal of Agronomy*, *18*(3–4), 235–265. https://doi.org/10.1016/S1161-0301(02)00107-7<./bib>

Kanzari, S., Nouna, B. B., Mariem, S. B., & Rezig, M. (2018). Hydrus-1D model calibration and validation in various field conditions for simulating water flow and salts transport in a semi-arid region of Tunisia. *Sustainable Environment Research*, *28*(6), 350–356. https://doi.org/10.1016/j.serj.2018.10.001

Karandish, F., & Šimůnek, J. (2019). A comparison of the HYDRUS (2D/3D) and SALTMED models to investigate the influence of various water-saving irrigation strategies on the maize water footprint. *Agricultural Water Management*, *213*, 809–820. https://doi.org/10.1016/j.agwat.2018.11.023

Karra, Y., Boujghagh, M., Serghini, M. A., & Lage, M. (2017). Effect of planting density on productivity of saffron corms. In M. Lage, C. Al Faiz, & M. Badraoui (Eds.), *V International Symposium on Saffron Biology and Technology: Advances in Biology, Technologies, Uses and Market* (pp. 119–124). ISHS Acta Horticulturae. https://www.actahort.org/books/1184/1184_17.htm

Kassaye, K. T., Boulange, J., Saito, H., & Watanabe, H. (2021). Soil water content and soil temperature modeling in a vadose zone of Andosol under temperate monsoon climate. *Geoderma*, *384*, Article 114797. https://doi.org/10.1016/j.geoderma.2020.114797

Kendall, M. G. (1975). *Rank correlation methods*. Griffin.

Khaliq, A., Tahir, M. M., Awan, S. I., & Shaheen, A. (2024). Growth, yield and quality of Saffron in response to different soil textures and temperature regimes. *Soil Environment*, *42*(2), 243380. https://doi.org/10.25252/SE/2024/243380

Kodešová, R., Fér, M., Klement, A., Nikodem, A., Teplá, D., Neuberger, P., & Bureš, P. (2014). Impact of various surface covers on water and thermal regime of Technosol. *Journal of Hydrology*, *519*, 2272–2288.

Koocheki, A., Ganjali, A., & Abbassi, F. (2007). The effect of duration of incubation and photoperiod on corm and shoot characteristics of saffron plant (*Crocus sativus* L.). *Acta Horticulturae*, *739*, 61–70. https://doi.org/10.17660/ActaHortic.2007.739.6

Koocheki, A., Khorramdel, S., & Banhangi, F. M. (2022). Effect of corm harvesting year on agronomic criteria, daughter corm, and flower yield of saffron (*Crocus sativus* L.). *Saffron Agronomy and Technology*, *10*, 101–116.

Koocheki, A., & Seyyedi, S. M. (2015). Relationship between nitrogen and phosphorus use efficiency in saffron (*Crocus sativus* L.) as affected by mother corm size and fertilization. *Industrial Crops and Products*, *71*, 128–137. https://doi.org/10.1016/j.indcrop.2015.03.085

Maraun, D., Wetterhall, F., Ireson, A. M., Chandler, R. E., Kendon, E. J., Widmann, M., Brienen, S., Rust, H. W., Sauter, T., Themeßl, M., Venema, V. K. C., Chun, K. P., Goodess, C. M., Jones, R. G., Onof, C., Vrac, M., & Thiele-Eich, I. (2010). Precipitation downscaling under climate change: Recent developments to bridge the gap between dynamical models and the end user. *Reviews of Geophysics*, *48*(3), Article RG3003. https://doi.org/10.1029/2009RG000314

Marquardt, D. W. (1963). An algorithm for least-squares estimation of nonlinear parameters. *Journal of the Society for Industrial and Applied Mathematics*, *11*(2), 431–441. https://doi.org/10.1137/0111030

Mehmeti, A., Candido, V., Canaj, K., Castronuovo, D., Perniola, M., D'Antonio, P., & Cardone, L. (2024). Energy, environmental, and economic sustainability of saffron cultivation: Insights from the first European (Italian) case study. *Sustainability*, *16*(3), Article 1179. https://doi.org/10.3390/su16031179

Mirsafi, Z. S., Sepaskhah, A. R., Ahmadi, S. H., & Kamgar-Haghighi, A. A. (2016). Assessment of AquaCrop model for simulating growth and yield of saffron (Crocus sativus L.). *Scientia Horticulturae*, *211*, 343–351. https://doi.org/10.1016/j.scienta.2016.09.020

Mohammadi, B., Guan, Y., Aghelpour, P., Emamgholizadeh, S., Pillco Zolá, R., & Zhang, D. (2020). Simulation of Titicaca lake water level fluctuations using hybrid machine learning technique integrated with grey wolf optimizer algorithm. *Water*, *12*(11), Article 3015. https://doi.org/10.3390/w12113015

Molina, R. V., Valero, M., Navarro, Y., Guardiola, J. L., & Garcia-Luis, A. J. S. H. (2005). Temperature effects on flower formation in saffron (*Crocus sativus* L.). *Scientia Horticulturae*, *103*(3), 361–379. https://doi.org/10.1016/j.scienta.2004.06.005

Moshizi, Z. G. N., Bazrafshan, O., Etedali, H. R., Esmaeilpour, Y., & Collins, B. (2023). Application of inclusive multiple model for the prediction of saffron water footprint. *Agricultural Water Management*, *277*, Article 108125. https://doi.org/10.1016/j.agwat.2022.108125

Nakhaei, M., & Šimůnek, J. (2014). Parameter estimation of soil hydraulic and thermal property functions for unsaturated porous media using the HYDRUS-2D code. *Journal of Hydrology and Hydromechanics*, *62*(1), 7–15. https://doi.org/10.2478/johh-2014-0008

Negm, A., Capodici, F., Ciraolo, G., Maltese, A., Provenzano, G., & Rallo, G. (2017). Assessing the performance of thermal inertia and Hydrus models to estimate surface soil water content. *Applied Sciences*, *7*(10), Article 975. https://doi.org/10.3390/app7100975

Nocedal, J. & Wright, S. J. (Eds.). (1999). *Numerical optimization*. Springer. https://doi.org/10.1007/b98874

O'Neill, B. C., Tebaldi, C., Van Vuuren, D. P., Eyring, V., Friedlingstein, P., Hurtt, G., Knutti, R., Kriegler, E., Lamarque, J.-F., Lowe, J., Meehl, G. A., Moss, R., Riahi, K., & Sanderson, B. M. (2016). The scenario model intercomparison project (ScenarioMIP) for CMIP6. *Geoscientific Model Development*, *9*(9), 3461–3482. https://doi.org/10.5194/gmd-9-3461-2016

Pirasteh-Anosheh, H., Babaie-Zarch, M. J., Nasrabadi, M., Parnian, A., Alavi-Siney, S. M., Beyrami, H., & Race, M. (2023). Climate and management factors influence saffron yield in different environments. *Agrosystems, Geosciences & Environment*, *6*(3), e20418.

Rastegaripour, F., Tavassoli, A., Babaeian, M., Fernández-Gálvez, J., & Caballero-Calvo, A. (2024). Assessing the impacts of climate change on water resource management and crop patterns in Eastern Iran. *Agricultural Water Management*, *295*, Article 108774. https://doi.org/10.1016/j.agwat.2024.108774

Renau-Morata, B., Nebauer, S. G., García-Carpintero, V., Cañizares, J., Minguet, E. G., De los Mozos, M., & Molina, R. V. (2021). Flower induction and development in saffron: Timing and hormone signalling pathways. *Industrial Crops and Products*, *164*, Article 113370. https://doi.org/10.1016/j.indcrop.2021.113370

Rezvani-Moghaddam, P. (2020). Ecophysiology of saffron. In A. Koocheki & M. Khajeh-Hosseini (Eds.), *Saffron: Science, technology and health* (pp. 119–137). Elsevier. https://doi.org/10.1016/B978-0-12-818638-1.00008-3

Richards, F. J. (1959). A flexible growth function for empirical use. *Journal of Experimental Botany*, *10*(2), 290–301. https://doi.org/10.1093/jxb/10.2.290

Ritchie, J. T. (1972). Model for predicting evaporation from a row crop with incomplete cover. *Water Resources Research*, *8*(5), 1204–1213. 10.1029/WR008i005p01204

Selahvarzi, M., Naghedifar, S. M., Oliazadeh, A., & Loáiciga, H. A. (2025). Hierarchical pseudo-continuous machine-learning-based pedotransfer models for infiltration curves: An investigation on the role of regularization and ensemble modeling. *Journal of Hydrology*, *650*, Article 132459. https://doi.org/10.1016/j.jhydrol.2024.132459

Sepaskhah, A. R., Amini-Nejad, M., & Kamgar-Haghighi, A. A. (2013). Developing a dynamic yield and growth model for saffron under different irrigation regimes. *International Journal of Plant Production*, *7*(3), 437–504.

Sepaskhah, A. R., & Kamgar-Haghighi, A. A. (2009). Saffron irrigation regime. *International Journal of Plant Production*, *3*(1), 1–16.

Sharafkhane, M. G., Ziaei, A. N., Naghedifar, S. M., Akbari, A., & Verdi, A. (2024). AquaCrop Plug-in-PSO: A novel irrigation scheduling optimization framework for maize to maximize crop water productivity using in-season weather forecast and crop yield estimation. *Agricultural Water Management*, *306*, Article 109153. https://doi.org/10.1016/j.agwat.2024.109153

Šimůnek, J., van Genuchten, M. Th., & Šejna, M.(2007). Modeling subsurface water flow and solute transport with HYDRUS and related numerical software packages. In *Numerical modelling of hydrodynamics for water resources* (pp. 107–126). CRC Press.

Šimůnek, J., & Hopmans, J. W. (2002). Parameter optimization and nonlinear fitting. In J. H. Dane & G. C. Topp (Eds.), *Methods of soil analysis: Part 4 physical methods* (Vol. 5, 139–157). SSSA.

Šimůnek, J., Šejna, M., Saito, H., Sakai, M., & van Genuchten, M. Th. (2008). The Hydrus-1D Software Package for Simulating the Movement of Water, Heat, and Multiple Solutes in Variably Saturated Media (Version 4.0) [HYDRUS Software Series 3]. Department of Environmental Sciences, University of California, Riverside.

Šimůnek, J., & Suarez, D. L. (1993). Modeling of carbon dioxide transport and production in soil: 1. Model development. *Water Resources Research*, *29*(2), 487–497.

Šimůnek, J., & van Genuchten, M. T. (2008). Modeling nonequilibrium flow and transport processes using HYDRUS. *Vadose Zone Journal*, *7*(2), 782–797.

Šimunek, J., Van Genuchten, M. T., & Šejna, M. (2012). HYDRUS: Model use, calibration, and validation. *Transactions of the ASABE*, *55*(4), 1263–1274. https://doi.org/10.13031/2013.42239

Steduto, P., Hsiao, T. C., Raes, D., & Fereres, E. (2009). AquaCrop—The FAO crop model to simulate yield response to water: I. Concepts and underlying principles. *Agronomy Journal*, *101*(3), 426–437. https://doi.org/10.2134/agronj2008.0139s

Stöckle, C. O., Donatelli, M., & Nelson, R. (2003). CropSyst, a cropping systems simulation model. *European Journal of Agronomy*, *18*(3–4), 289–307.

Themeßl, M. J., Gobiet, A., & Heinrich, G. (2012). Empirical-statistical downscaling and error correction of regional climate models and its impact on the climate change signal. *Climatic Change*, *112*(2), 449–468.

Van Diepen, C. V., Wolf, J. V., Van Keulen, H., & Rappoldt, C. (1989). WOFOST: A simulation model of crop production. *Soil Use and Management*, *5*(1), 16–24.

Van Genuchten, M. T. (1980). A closed-form equation for predicting the hydraulic conductivity of unsaturated soils. *Soil Science Society of America Journal*, *44*(5), 892–898.

Van Genuchten, M. V., Leij, F. J., & Yates, S. R. (1991). *The RETC code for quantifying the hydraulic functions of unsaturated soils* (Version 1.0 EPA Rep. 600/2-91/065). U.S. Salinity Laboratory, USDA-ARS.

Ventrella, D., Castellini, M., Di Prima, S., Garofalo, P., & Lassabatère, L. (2019). Assessment of the physically-based HYDRUS-1D model for simulating the water fluxes of a Mediterranean cropping system. *Water*, *11*(8), Article 1657.

Wang, X., Li, Y., Chau, H. W., Tang, D., Chen, J., & Bayad, M. (2021). Reduced root water uptake of summer maize grown in water-repellent soils simulated by HYDRUS-1D. *Soil and Tillage Research*, *209*, Article 104925. https://doi.org/10.1016/j.still.2020.104925

Wang, Z., Li, X., Xu, J., Yang, Z., & Zhang, Y. (2021). Effects of ambient temperature on flower initiation and flowering in saffron (*Crocus sativus* L.). *Scientia Horticulturae*, *279*, Article 109859.

Williams, J. R., Jones, C. A., Kiniry, J. R., & Spanel, D. A. (1989). The EPIC crop growth model. *Transactions of the ASAE*, *32*(2), 497–0511. https://doi.org/10.13031/2013.31032

Wu, L., Tian, J., Liu, Y., Wang, Y., & Zhang, P. (2024). Multi-objective planting structure optimisation in an irrigation area using a grey wolf optimisation algorithm. *Water*, *16*(16), Article 2297. https://doi.org/10.3390/w16162297

Yadav, B., Krishnan, P., Shafeeq, P. M., Parihar, C. M., & Aggarwal, P. (2020). Modelling soil thermal regime in wheat using HYDRUS-2D under diversified maize-wheat-mungbean cropping system. *Catena*, *194*, Article 104765. https://doi.org/10.1016/j.catena.2020.104765

Yarami, N., & Sepaskhah, A. R. (2015). Saffron response to irrigation water salinity, cow manure and planting method. *Agricultural Water Management*, *150*, 57–66. https://doi.org/10.1016/j.agwat.2014.12.004

Yi, J., Li, H., Zhao, Y., Zhang, H., & Liu, M. (2022). Assessing soil water balance to optimize irrigation schedules of flood-irrigated maize fields with different cultivation histories in the arid region. *Agricultural Water Management*, *265*, Article 107543. https://doi.org/10.1016/j.agwat.2022.107543

Zamani, A., Sharifi, A., Felegari, S., Tariq, A., & Zhao, N. (2022). Agro climatic zoning of saffron culture in miyaneh city by using WLC method and remote sensing data. *Agriculture*, *12*(1), 118.

Zhang, R., Zhu, M., Mady, A. Y., Huang, M., Yan, X., & Guo, T. (2024). Effects of different long-term fertilization and cropping systems on crop yield, water balance components and water productivity in dryland farming. *Agricultural Water Management*, *292*, Article 108689. https://doi.org/10.1016/j.agwat.2024.108689

Zhuo, W., Fang, S., Wu, D., Wang, L., Li, M., Zhang, J., & Gao, X. (2022). Integrating remotely sensed water stress factor with a crop growth model for winter wheat yield estimation in the North China Plain during 2008–2018. *The Crop Journal*, *10*(5), 1470–1482. https://doi.org/10.1016/j.cj.2022.04.004

How to cite this article: Akbari, A., Ziaei, A. N., Naghedifar, S. M., Hopmans, J. W., & Gholipour, J. (2025). Modeling saffron corm production under climate change using Hydrus-1D enhanced with a novel crop yield module. *Vadose Zone Journal*, *24*, e70056. https://doi.org/10.1002/vzj2.70056